Investigating Mono– and Quadrupole Gravitational Light Deflection by Jupiter

Adriaan-Alexander Ludl

Lund Observatory
Lund University

2011-EXA57

Degree project of 15 higher education credits
September 2011

Lund Observatory
Box 43
SE-221 00 Lund
Sweden

Investigating Mono– and Quadrupole Gravitational Light Deflection by Jupiter

Adriaan-Alexander Ludl[1,2]

Supervisors: David Hobbs[1] and Lennart Lindegren[1]

[1]Department of Astronomy and Theoretical Physics,
Lund University, Lund, Sweden

[2]Institut Supérieur de l'Aéronautique et de l'Espace,
Formation Supaéro, Toulouse, France

Abstract

Gravitational light deflection in the Solar System can be detected by high precision astrometric measurements. We discuss the parametrized post-Newtonian framework and the comparison of metric theories of gravity. At the precision of a few micro-arcseconds, Gaia data will permit tests of the PPN parameters β and γ and to distinguish monopole and quadrupole gravitational light deflection. Accounting for relativistic effects is necessary to achieve the aimed for precision. The theoretical formulation of light deflection is discussed. We deduce an expression for the source direction derivatives required by the AGIS scheme in a simplified relativistic model. This model accounting for monopole and quadrupole deflection terms has been implemented in AGISLab. We have validated the implementation and maintain convergence of the astrometric solution for Gaia.

Contents

« ubi materia, ibi geometria »

Johannes Kepler's Thesis XX from
De fundamentis astrologiae certioribus

1 Introduction

Determining the positions and motions of stars and other stellar objects with ever greater precision has been a task of paramount importance in astronomy over thousands of years and has spawned manifold discoveries. The study of kinematic and dynamic properties of stars has allowed a deeper understanding of their physical properties such as their spectra and their sizes. The Gaia satellite mission will be an astrometric survey of one billion stars at a precision of a few micro-arcseconds. We here discuss the influence of gravitational light deflection on the data reduction for Gaia and how this can be used as a test of general relativity and competing theories.

Measurement of gravitational light deflection by the Sun and the planets of the solar system constitutes a test of general relativity and its extensions. All light deflection measurements to date only allow to confirm the correctness of the monopole light deflection predicted by general relativity. The quadrupole light deflection however has not yet been measured. It serves as a test of General Relativity and other contending theories of gravitation.

1.1 Scope of this work

The objective of this six months project is to simulate gravitational light deflection by the Sun and the planets of the solar system and to study the detection of these effects by the Gaia mission. The goal is to determine the possibility to constrain post Newtonian models of gravity.

In section 2 we present the astrometric problem in the context of the Gaia mission. We describe its main features which will make it possible to achieve the aimed for precision.

We will discuss the equations of gravitational light deflection in section 3. The theoretical foundations and experimental evidence leading to general relativity and competing theories of gravity are examined. Then the parametrized post Newtonian framework described in Will [1993] is introduced. It allows for the predictions of general relativity and other metric theories to be compared.

The appendices give acronyms and notations, units and quote the full parametrized post-Newtonian framework as described by Will [2006].

2 Astrometry

2.1 Historical overview of astrometry

What is astrometry? Astrometry is the discipline concerned with the study and measurement of the kinematic and dynamic properties, and the brightness (magnitude) of celestial bodies. Among those properties are the positions and motions of objects, as well as their size [Kovalevsky, 2002]. The development of astronomy and astrometry is tightly linked to the compilation of star catalogues. They can be traced back to Timocharis, Aristillus and Hipparchus in the second century BC, and have gradually increased in size. Their form has changed from hand written recordings on papyrus or paper to globally accessible digital databases such as Simbad. Today these are updated daily and incorporate data from satellite missions such as HIPPARCOS.

A catalog provides the identification of stars and their positions. This allows one to track the motion of stars and the evolution of their physical characteristics. [Perryman, 2010]

The increase in precision of measurements has spawned discoveries of new phenomena and objects, such as the precession of orbits, the structure of the galaxy, the motion of the Sun around the center of the Milky Way galaxy, and the discovery of other galaxies.

The kinematic properties are the positions and motions of the planets. The sky is usually mapped by a spherical coordinate system consisting of two angles describing an object's orientation on the sky and the third coordinate being the distance to the origin. The proper motion of an object is the variation of these three parameters. A more detailed discussion of coordinate systems and reference frames can be found below.

The dynamic properties are found from the variations in the time series of observations. They are described by their apparent acceleration. The precise determination of all of these needs careful transformation between different reference frames to take into account relativistic effects.

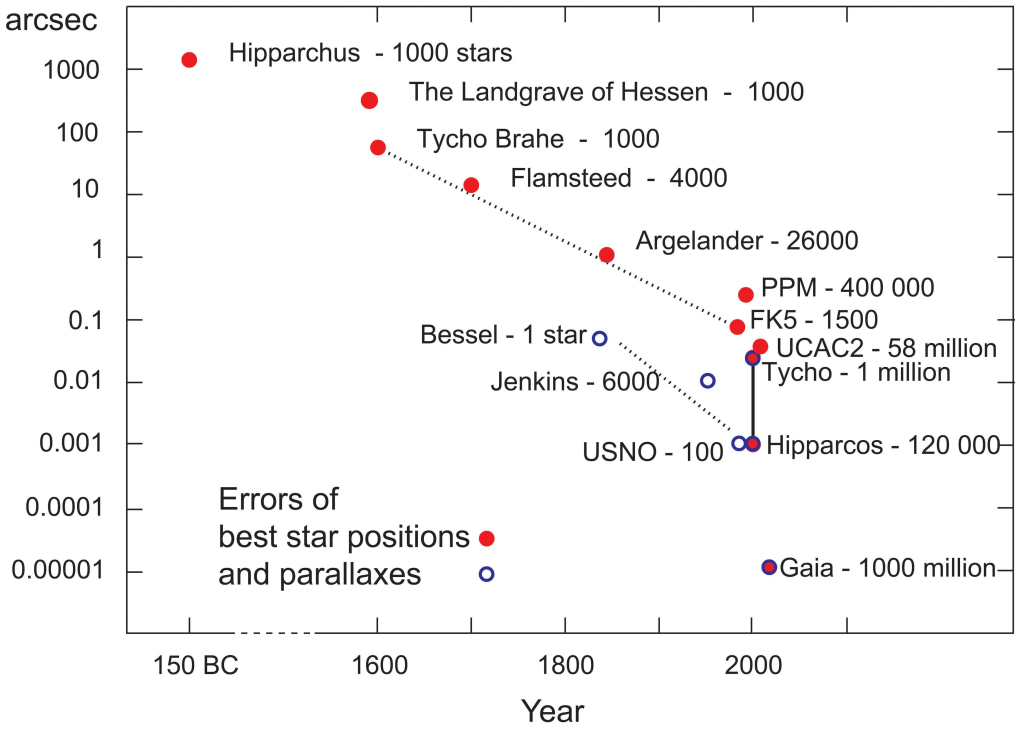

Figure 1: Diagram illustrating the progress in astrometric accuracy from Hipparchus to Gaia. The latter space astrometry mission will push astrometric measurements to the limits. (Jos de Bruijne, 2009, ESA Science Team [2010] [2])

Objects studied in astrometry Star maps and catalogs describe the positions and motions of celestial objects. To give but a brief overview of the different kinds of objects, a more detailed one can be found in most modern astronomy textbooks (for instance Kovalevsky [2002]).

- planets : "wandering" objects which move quickly compared to an apparently fixed background
- stars : on short time scales these appear to be fixed on the celestial sphere and are small and possibly bright objects. They are self gravitating balls of gas.
- diffuse objects such as nebulae, clusters, galaxies which may be composed of hot gas, dust, or large numbers of stars

The Milky Way has three structural components: the flat disc, the bulge and the halo. The flat disc contains nearly 10^{11} stars of all spectral types and ages orbiting the Galactic centre. The bulge is less flattened, supposedly contains a supermassive black hole and may contain a bar. The halo surrounds the disc and bulge, has roughly 10^9 stars, which are old and metal poor, as well as approximately 160 globular clusters and a small number of satellite dwarf galaxies. This entire system is embedded in a massive halo of dark material of unknown composition and poorly known spatial distribution [Jos de Bruijne, GAIA: Galactic Structure in Gaia Infosheet 2009][2]. The internal physical properties of these objects are not the subject of study of astrometry and will not be further discussed here.

The main concern of astrometry is the precise measurement of positions and motions of these objects. These are expressed in a reference frame. The sky is mapped by a spherical coordinate system consisting of two angles describing an object's orientation on the sky and the third coordinate being the distance to the origin. This is discussed in in further detail in section 3.2.4.

Astrometry and relativity In the history of scientific thought considerable effort has gone into devising a simple elegant description and model of planetary motion. The Keplerian revolution and Newton's law of gravitation provided a unified framework for astrometric calculations and provided a basis for new discoveries. The ideas at the heart of special and general relativity originate in the same search for a simple geometrical description of reality on all scales. These theoretical frameworks have allowed to explain phenomena which had hitherto remained mysterious such as the perihelion precession of Mercury. The latter is a small effect ($43''$ per century) and highly accurate instruments and techniques are required to obtain precise measurement.

The main principle of relativistic theories is the principle of equivalence, which contains the assumption of constant speed of light. This will be further discussed in section 3.2.1.

The ties between astrometry and relativity lie in the experiments. Today's precise astrometric measurements require models which take into account relativistic effects. This in turn allows to test the predictions of special and general relativity. The Eddington experiment performed during the 1919 solar eclipse measured the light bending by the Sun. It was one of the first tests of the general theory of relativity, although the quality of the data has been the subject of dispute. Today the improvements in experimental techniques have allowed to place constraints on the validity of general relativity and to test its predictions against those of alternative theories. The upcoming Gaia mission will survey the sky and permit tests of general relativity to higher precision. One of these is the measurement of gravitational light deflection by Jupiter which is the subject of this project.

[2] `http://www.rssd.esa.int/index.php?project=GAIA&page=Info_sheets_overview`

Hipparcos and subsequent catalogs Earth bound astrometry was limited by effects such as atmospheric variability and seismic perturbations. The motivation behind the Hipparcos mission was to lift these limits by making high precision astrometry space-borne to avoid these limitations.

Hipparcos (High Precision Parallax Collecting Satellite) was a satellite mission of the European Space Agency during the 1990's. It produced a three-dimensional map of the sky. The first catalog produced using this data, the Hipparcos catalog contains 117 955 stars with astrometric data. The positions are accurate to better than 2 milli arcseconds, which is about a factor 100 better than can be obtained from Earth based observatories. The project also produced the Tycho catalog. It is more complete since it contains more than two million additional stars, but their astrometric data is less precise. [Perryman, 2010]

2.2 Gaia and current missions

2.2.1 The Gaia mission

The ESA mission Gaia has been designed with a view to survey our galaxy, the Milky Way. It will yield a star catalog with a precision of 8–25 μarcsec(μas) and will encompass stars down to magnitude 20 [Prusti, 2011]. Originally GAIA was an acronym for: Global Astrometric Interferometer for Astrophysics. As the mission has increased in complexity and different choices in technological implementation have been made, this has become obsolete. The idea of the mission was originally outlined in Lindegren et al. [1992] as a successor to ESA's Hipparcos mission. The mission was approved by ESA in 2000. The launch is planned for 2013 and the five years of observations are to start by 2014. The nominal duration of the mission is five years.

The scientific objectives of the Gaia mission are far reaching. The study of the Milky Way galaxy and its origin lie at their heart. Aside from the study of galaxy formation and galactic dynamics, it will provide statistics on many stars and thereby help to improve the understanding of stellar physics and evolution. The objects to be detected are also expected to be of all classes of astrophysical objects including brown dwarfs, white dwarfs, and planetary systems. The Gaia mission will also allow us to carry out a new Solar System census. Moreover the results of Gaia will contribute to the understanding of fundamental physics. In particular, high precision astrometry, that is precise angular distance and motion measurements will allow us to test General Relativity against competing theories of gravitation, which can be expressed in the parametrized post-Newtonian formalism (PPN gamma). This is discussed in more detail in section 3.2.3.

It will deliver a catalogue of about one billion stars in the Milky Way galaxy down to magnitude 20. The expected precision will allow to improve the distance scale of the Galaxy and the universe. It is expected that this will result in a three dimensional structural map of one billion stars in our galaxy, an improvement on the Hipparcos catalog by a factor of about ten thousand.

2.2.2 The Gaia satellite

Mechanics and orbit: The main structural element of Gaia is the silicon carbide torus, on which the instruments are mounted. The satellite will be in orbit around the Lagrange point L_2 of the Sun-Earth system. Its orbit is designed to allow it to scan the whole sky such that every object will be observed about 70 times.

- spinning on its axis at 6h for a full circle
- spin axis precessing a full circle in 63 days
- the orbital motion around the Sun in one year

These three motions allow an almost homogeneous coverage of the sky. On average 70 observations per source over the five year mission will be obtained.

At the second Lagrange point (L_2) Gaia will be in a nearly periodic Lissajous orbit, which is stable and avoids the need for large maneuvres. Small maneuvres will be required roughly one a month. This orbit also helps to avoid the eclipse zone during the mission. This is essential for the solar panels that generate power, and to keep the thermal environment stable. The selection of the orbit arose from a trade-off between communication, operations, cost, thermal and radiation environment, and accessibility with current rockets.

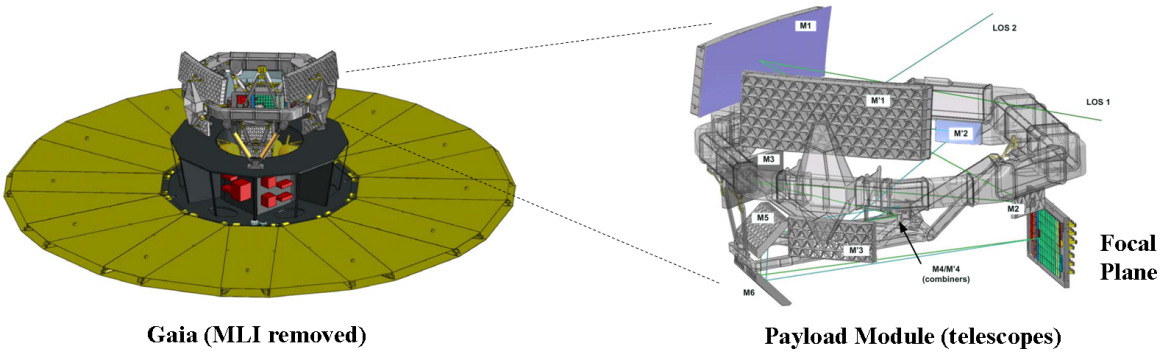

Figure 2: At the left, overview of the Gaia satellite showing the space craft and payload on top. A zoom on the payload module at the right shows the two main mirrors $M1$ and $M1'$ and focal plane (Copyright ESA).

Optics and detectors: There are three instruments in the payload on board Gaia. They will carry out astrometry, photometry and spectroscopy.

Here we shall give a brief overview of the science that the photometry and spectroscopy instruments will do and the general error requirements. Gaia will observe in the visual spectrum, in the magnitude range from 6 to 20. For astrometry the precision of the data will depend on the magnitude of the star. The parallax error is to be around 7 μarcsec for the brightest stars ($G < 13$)[3], 20μas (microarcseconds) at 15 mag, and 200μas at 20 mag. The photometric instrument will allow the determination of stellar surface parameters. It is designed to give temperatures to a few hundred Kelvin, gravities and metallicities to 0.2 dex. Thus the requirements on its sensitivity are: 8 to 20 mmag for a 15 mag star. The spectroscopic instrument is necessary for the determination of radial velocities of objects. It is designed for a precision better than 1 km/s for bright stars (V<13.5 mag), covering wavelengths from 330 to 1000 nm. The signal to noise ratio (S/N) of the spectroscopic instrument is required to be at resolution

[3]Here we use G to denote Gaia magnitudes. The definition of G and the transformation to other magnitude scales, is beyond the scope of this work. They are discussed briefly in Bastian [2007], and more extensively in Jordi et al. [2010].

better than $\Delta\lambda/\lambda = 10\,000$ for deduction of astrophysical parameters for a subsample of the sources [Prusti, 2011].

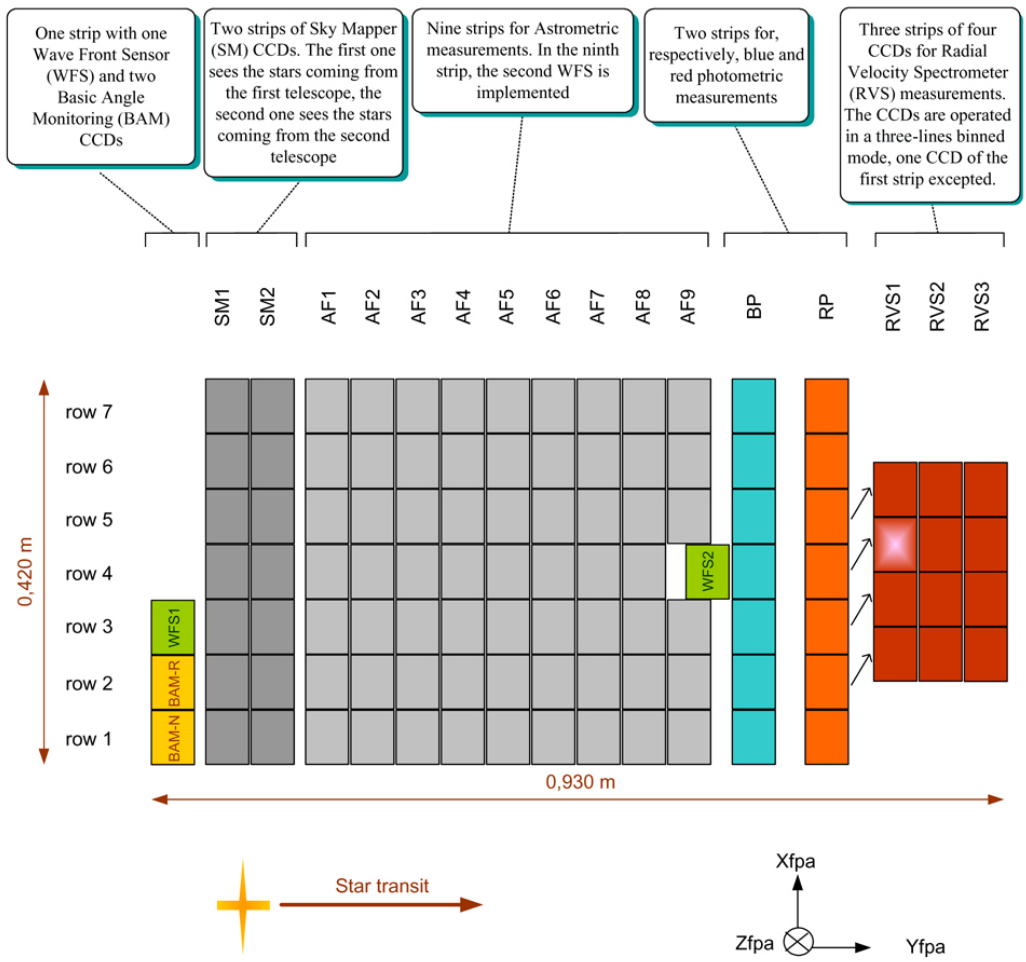

Figure 3: This diagram shows the CCD layout in focal plane of Gaia, with the astrometric field in light gray at the center. (Copyright EADS Astrium)

2.2.3 Limitations of the Gaia mission

There are technical limitations to the data Gaia will deliver. One of these is related to the filters used, they determine the observable wavelengths.

According to [Prusti, 2011] the problems are mainly of the following types. It is difficult to meet the astrometric precision requirements for blue stars, the reference star is B1V and the deviation is about 10% for the parallax error. Another class of stars that have high errors are those of magnitude $G < 7$ mag, the parallax requirement is missed by 1 to 2μarcsec. This is determined by the gating scheme used in the mission. Another problem is saturation of the CCDs by bright objects, Jupiter has V magnitude in the range of $[-3, -1.6]$ and its angular size is about 40 arcsec. This will result in a temporary blinding of the CCDs and make observations impossible within 5 arcsec of Jupiter. This is an important factor in the measurement of light deflection, mostly for the quadrupole (and weaker) terms [Hobbs et al., 2010, Martin Fleitas et al., 2011]. Additionally there are optical limitations such as the size of the mirrors and CCDs.

How far away can Gaia see into the Milky Way? This depends not only on the technical characteristics, but also on the extinction coefficients of interstellar matter and the direction

in which it is pointed. Distant objects can be seen if they are very bright or magnified by a gravitational lens for instance. What can be ascertained more clearly is the expected fraction of stars/objects/sources in the Milky Way that will be covered by the telescope. Approximately a billion objects in the magnitude range between 6 and 20, this corresponds only to 1% of all objects in the galaxy.

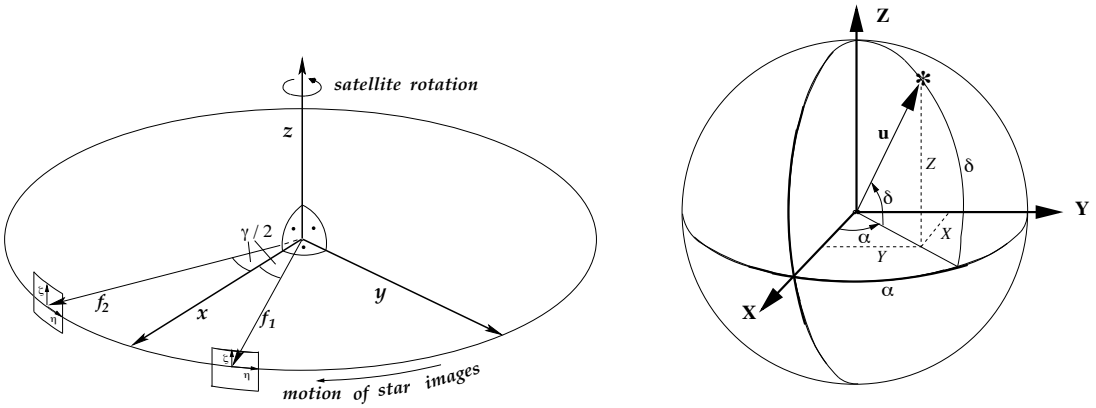

(a) The Scanning Reference System (SRS), the Gaia viewing directions and the Field-of-View Reference Systems (FoVRS). The angles between the two viewing directions are not drawn to scale. The black dots near the centre denote 90°angles (marked by the arcs). The big ellipse indicates the instantaneous scan great circle on the celestial sphere. The small rectangles indicate the fields on the sky; the small arrows show the orientation of the field angles. The principal axes f_1, f_2 of the FoVRS point towards the centre of each field of view. The w and z axes (not labeled in the diagram) point parallel to the η and ζ axes, respectively. The direction to the sun is always at an angle of 45°from the positive z axis.

(b) Illustrative sketch of the celestial sphere indicating the ICRS spherical coordinates (α, δ) and direction cosines (X, Y, Z) of a unit vector u towards a star (upper right), with the origin of (α, δ) at front left and the ICRS north pole towards the top.

Figure 4: The satellite and ICRS frames, both from Bastian [2007]

2.2.4 Scanning space astrometry

Scanning space astrometry is the term designating the kind of astrometric observation used in the Hipparcos and Gaia missions. It relies on the transformation between (linear) positional data and the spinning telescope. We will give an overview here, a detailed account can be found in Lindegren and Bastian [2011] and references therein.

Indeed, as Gaia will be scanning the sky, the precise time when the centre of a star image has some well-defined position in the field of view (FoV) is determined. The position is defined by the pixel layout of the CCDs in Gaia. Then the observation time is the one-dimensional (along-scan, AL) measurement of the stellar position relative to the instrument axes. At the same time an approximate across-scan (AC) position of the star is also measured. However, the AC measurement is less accurate due to the geometry of the CCDs which are elongated in the AC direction, the lower optical resolution across-scan, and the way the pixels are read out. The astrometric catalogue is produced after processing a very large number of such observation times. This process involves a precise reconstruction of the instrument pointing (attitude) as a function of time and of the optical mapping of the CCDs through the telescope onto the celestial sphere.

A number of factors impact the AL measurement. We will discuss the basic angle, the scanning law and parallax determination in the following.

Gaia's two fields of view (FoV) coincide on the focal plane shown in figure 3. The basic angle between them is Γ =106.5°. This choice is motivated by two reasons. The first is to make it as large as possible, the second to avoid divisors of 360°. The accuracy of the one-dimensional AL position measurement depends on the basic angle. In the 1D case there are peaks in the variance of star positions for basic angle values of the kind $\Gamma = m/n$ (rad) with m, n being small integers. These peaks should be avoided. In the case of Gaia we have $m = 71$ and $n = 240$, which are large enough to avoid such problems. It can be noted that this effect disappears for two dimensional measurements when the global solution over the whole celestial sphere is considered. Basic angle variations are unavoidable and have to be monitored, to compensate for the errors they could induce. This should be precise to within 10μarcsec, and will be monitored and measured down to 1μarcsec.

The scanning law describes the attitude of the satellite as a function of time. It gives the transformation between the Gaia proper frame and the reference frame for the catalog (e.g. BCRS). It prescribes the precession rate, the direction of the spin axis $\mathbf{z}$ as a function of time, the spin rate, which for Gaia is $60''s^{-1}$, the phase of the spin at some initial epoch, and solar aspect angle $\xi = 45°$.

To optimize the parallax measurement, large ξ are preferred, however protecting the satellite optics from direct and indirect sunlight imposes the constraint $\xi \leq 45°$. The chosen fixed value is also a factor that contributes to the constant thermal environment.

The spin period of Gaia is $P = 6$hr, the AC size of the FoV is $\Phi = 0.69°$. Preferably the areas of the sky scanned in successive spins should overlap, to avoid the occurrence of gaps. Therefore $|\mathbf{z}| \leq \Phi$ should be verified. This condition is not quite satisfied for Gaia, so there will be gaps. The precession rate is the inverse of the number of loops per year $K = 5.8$ for Gaia.

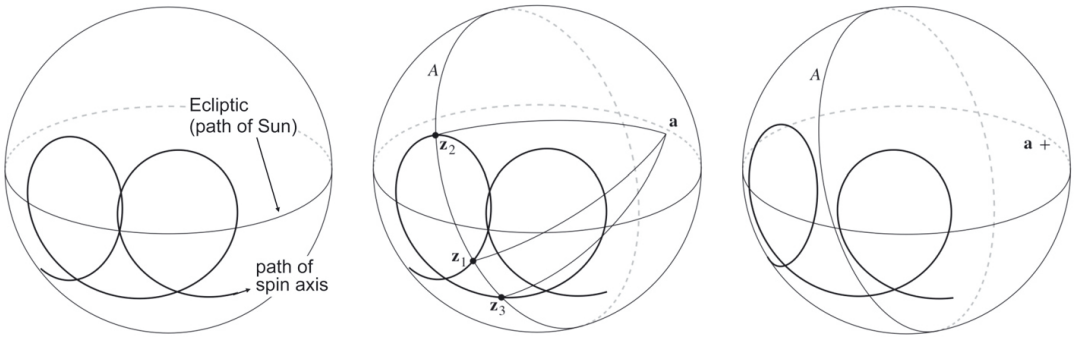

Figure 5: The precession of Gaia's spin axis, from [Lindegren and Bastian, 2011]. The spin axis $\mathbf{z}$ makes loops around the Sun, which must overlap as in the left and middle diagram in order to provide good observing conditions. The star at point $\mathbf{a}$ may be scanned whenever $\mathbf{z}$ is 90° from $\mathbf{a}$, that is on the great circle A at $\mathbf{z_1}, \mathbf{z_2}, \mathbf{z_3}$ and so on.

The resulting "uniform revolving scanning law" is the baseline for both Hipparcos and Gaia, with slightly different parameters.

Lindegren and Bastian [2011] have pointed out that absolute parallaxes are obtained, even though scanning space astrometry also makes purely differential measurements. The principle of the parallax measurement is illustrated in figure 6. In Lindegren and Bastian [2011] this is explained as follows. This is made possible by the measurement of the relative parallax shifts between stars at large angular separations. For an observer at 1 AU from the Sun, the apparent shift of a star due to its parallax ϖ equals $\varpi \sin\theta$ and is directed on a great circle from the star towards the Sun. As shown in Figure 6 (left), the AL parallax shift of the star at F is $\varpi_F \sin\theta \sin\psi = \varpi_F \sin\xi \sin\Gamma$, where $\xi = 45°$ is the constant solar aspect angle (between the Sun and the spin axis). At the same time the AL parallax shift of the star at P is zero.

The AL measurement of F relative to P therefore depends on ϖ_F but not on ϖ_P, while the reverse is true at a different time, as shown in the right diagram.

The sensitivity to parallax is proportional to $\sin\xi \sin\Gamma$, which should therefore be maximized. The choice of ξ was discussed above. While $\Gamma = 90°$ is optimal for the basic angle according to this analysis, we have seen that other considerations led to a slightly larger value being adopted for Gaia.

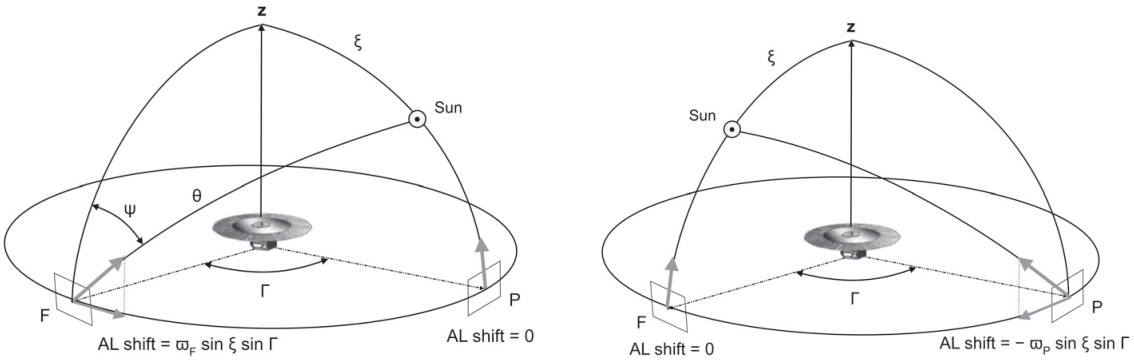

Figure 6: The geometry of the parallax measurement: The measured along-scan (AL) angle between the stars at P, F depends on their parallaxes ϖ_P, ϖ_F in different ways depending on the position of the Sun. This allows to determine their absolute parallaxes rather than just the relative parallax $\varpi_P - \varpi_F$. [Lindegren and Bastian, 2011].

This is relevant to the study of light deflection because the monopole deflection of the Sun is similar to a global shift of the parallaxes [Hobbs et al., 2010].

The parallax shift of a star is directed toward the Sun, as shown by the arrows on F and P in figure 6. The monopole light deflection is a shift of the apparent position of the star away from the Sun (along the great circle). In figure 6 the angle between the Sun and the star F along the great circle is θ. This effect has been shown to result in a statistical correlation of PPN γ and the parallax zero point [Mignard, 2002]. Both shifts have to be taken into account to determine the correct direction toward the star. These two shifts differ in their dependence on the angular separation from the Sun, this property is used in the data processing chain to distinguish them and determine the value of PPN γ for the Sun.

2.3 Data processing : AGIS, AGISLab and GREM

Gaia will produce a large amount of data, approximately 40Gb of telemetry data per day and an estimated 100 Tb over the 5 year mission. (Uwe Lammers, *Gaia: Astrometric Data Reduction* ESA Science Team [2010]) To cope with the data processing the Gaia Data Processing and Analysis Consortium (DPAC) has been formed in 2006 to structure the Gaia working groups and the efforts of the scientific community across Europe (M. Perryman, 2006, ESA Science Team [2010]). DPAC is in charge of the data reduction for Gaia. This comprises astrometric data reduction and the reduction of spectroscopic and photometric data. Among these are binary recognition, search for moving objects and exoplanets.

The main steps of the data processing chain are shown in figure 7. There are two phases the daily data processing and the Astrometric Global Iterative Solution (AGIS). The Initial Data Treatment (IDT) first processes the daily telemetry data, which evaluates the astrometric image parameters using the raw CCD data. The output of IDT is fed to the One Day Astrometric Solution (ODAS) which is part of Gaia's First-Look (FL) system. It evaluates the source parameters, the satellite's attitude and calibration parameters to sub-milli-arcsec accuracy. The daily results are then written into the Main Data Base (MDB). (Uwe Lammers, *Gaia: Astrometric Data Reduction* ESA Science Team [2010])

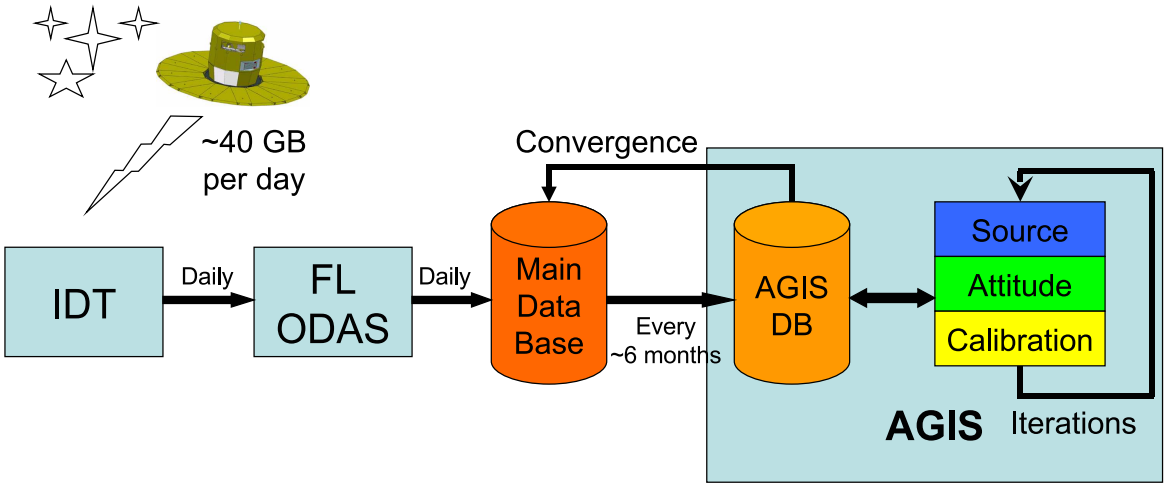

Figure 7: This diagram shows a schematic overview of the astrometric data processing chain for Gaia. The main units are IDT, FL-ODAS and AGIS which are described above. IDT and FL-ODAS perform preliminary evaluation of data and astrometric parameters. AGIS will generate the final astrometric mission products every six months and on the final data set. (Credit: Uwe Lammers ESA Science Team [2010])

2.3.1 AGIS and AGISLab

The MDB will accumulate data constantly, it is this data which is the input to AGIS, the core data processing module, which will analyse this data every 6 months. It produces a "Gaia catalog" with expected accuracies of 8–25 μarcsec (μas) for trigonometric parallaxes, positions at mean epoch and annual proper motions of simple stars[4] [Lindegren et al., 2011, p. 1] The subset of well-behaved primary stars is now believed to be substantially larger than 100 million [Lammers and Lindegren, 2011].

The determination of the "core solution" is an exceedingly difficult task, since there are very large quantities of data involved and due the complexity of the relationships between astrometric, spectroscopic and photometric data, as well as data collected at different epochs.

[4] i.e. apparently single stars

The astrometric core solution determines the five astrometric parameters for the primary stars. The direct resolution of the overdetermined problem involving about 10^{12} measurements and roughly $5 \cdot 10^9$ unknowns is unfeasible, despite the sparse nature of the matrix (figure 8). AGIS minimises the merit function χ in a least squares algorithm.

$$\chi^2(X) = \sum_i \frac{R_i(X)^2}{\sigma_i^2 + \epsilon_i^2} w \left(\frac{R_i(X)}{\sqrt{\sigma_i^2 + \epsilon_i^2}} \right) \tag{1}$$

where X is the vector containing the unknowns, i is the observation index, R_i the residuals, σ_i the formal observation certainty, ϵ_i the excess noise, and w the down-weighting function. This formula is discussed in Lammers and Lindegren [2011].

From equation (1) the standard system of normal equations for source, attitude and calibration parameters is deduced. This system can be solved by iterating in a straight forward way. In practice alternating phases of "Simple Iterations", "Accelerated Simple Iterations" and Conjugate Gradient iterations have been employed. There is a large number of unknowns, approximately: $5 \cdot 10^8$ source parameters, $4 \cdot 10^7$ attitude parameters and 10^6 calibration parameters. To this a small set of global parameters may be added [Lammers and Lindegren, 2011] (PPN γ is discussed in section 3.2.3). A global normal matrix can also be deduced when the global parameters are solved for, the global normal equation is given as equation (90) in Lindegren et al. [2011]. At least as many measurements as unknowns are needed to obtain an accurate solution. Consequently, AGIS will be executed only about once every 6 months, when enough data has been collected. This choice was made, considering the number of operations needed for the solution (expected to be some 10^{20} FLOPS) and the expected increase in precision achievable. One full run at the end of the mission is estimated to take about 2 months on a 10 TFLOP/s processing system. Further discussion of the complexity of the astrometric problem can be found in Bombrun et al. [2010].

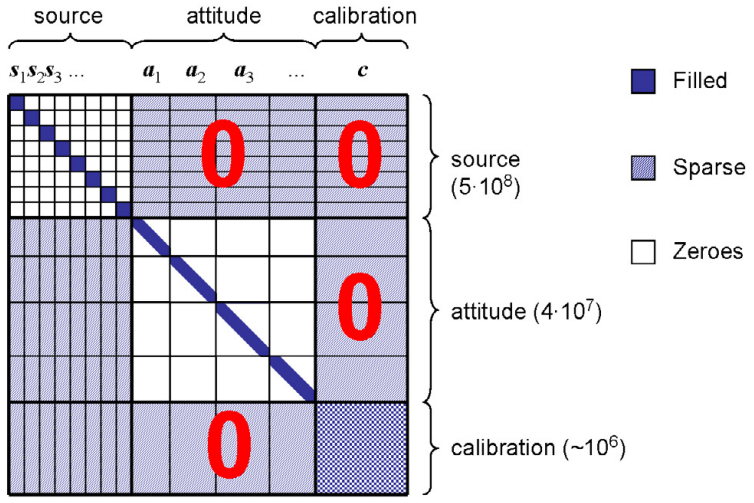

Figure 8: The structure of the normal equation matrix to be solved with AGIS. Setting four of the off-diagonal block to zero (red figures) gives the Gauss-Seidel pre-conditioner. Numbers in braces indicate the number of parameters of each kind. Lammers and Lindegren [2011]

AGISLab is a scaled version of AGIS developement mainly by Holl, Hobbs and Lindegren in Lund. It can run on less than 10^6 stars and therefore allows a significant number of Monte Carlo simulations with different noise realisations to be made in a relatively short time [Holl et al., 2010].

The scaling parameter is S, the simulations run in AGISLab use a fraction S of the total number of sources. AGISLab is designed to modify the Gaia layout in such a fashion that

certain quantities of interest for data analysis are conserved. This is achieved by reducing the focal length of the telescope and its spin rate, whereby "the mean number of stars in the focal plane at any time, the mean number of field transits of a given star over the mission, and the mean number of observations per degree of freedom of the attitude model " are conserved [Holl et al., 2010].

Building on the work in Hobbs et al. [2010], we have studied the possibilities of measuring light-deflection and PPN γ with Gaia by expanding the model for gravitational light deflection used in AGISLab.

2.3.2 Gaia relativity models

The resolution of the astrometric problem for Gaia, requires a consistent treatment of source parameters in a relativistic framework. As described in Crosta and Vecchiato [2010], there are currently two models that permit to obtain this solution with microarcsecond precision: GREM and RAMOD.

The baseline relativity model for Gaia is the Gaia Relativistic Model (GREM). This framework is built on the post-Newtonian approximation of metric theories of gravity[5] and the parametrized post-Newtonian formalism. It takes into account light deflection and other relativistic effects inside and outside the Solar System. These effects are treated as perturbations to the assumed solution (source direction) outside the Solar System [Crosta and Vecchiato, 2010, Klioner, 2003, 2008]. This is akin to the model we solve in the PPN formalism (see section 3.3.5).

The Relativistic Astrometric Model (RAMOD) follows a different approach. It solves the inverse ray tracing problem for general relativity. It is not constrained to approximations and this allows to probe the predictions of general relativity specifically. [Crosta and Vecchiato, 2010]

The advantage of GREM is that it allows to directly compare the different viable theories of gravitation and to place boundaries of the PPN parameters[6]. Both models are designed to be used for Gaia data reduction, thus is it essential that their results can be compared. Crosta and Vecchiato [2010] discuss a comparison between the two frameworks.

In the next section we will present a model of light deflection based on [Crosta and Mignard, 2006] and accounting for monopole and quadrupole light deflection. This model will be implemented into AGISLab to perform realistic numerical simulations of the astrometric solution on Gaia data. The quadrupole effect is also studied by the Gaia Relativistic Experiment on Quadrupole light deflection (GAREQ formerly GAREX). We believe that the comparison of our results to the preliminary results of these more complete models will prove to be beneficial.

[5] See section 3.2.1 for a definition of metric theories of gravity of which general relativity is one example.

[6] The parametrized post-Newtonianframework and parameters (PPN) are discussed in section 3.2.3

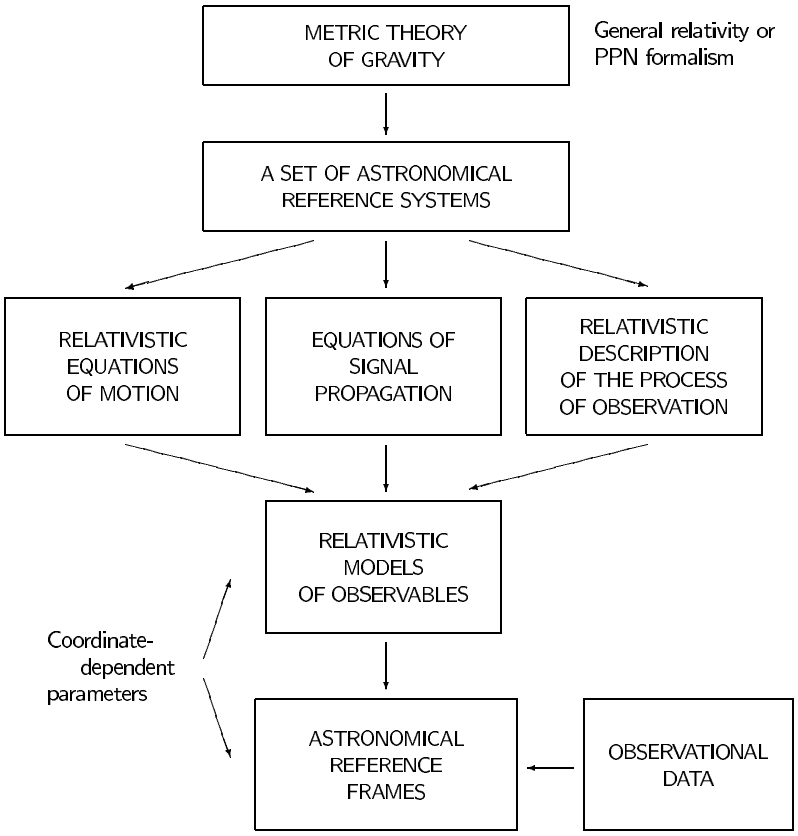

Figure 9: Representation of the general principles underlying the relativistic modeling of astronomical observations. Klioner [2003]

3 Gravitational light deflection

3.1 Light bending and experimental tests of relativity

3.1.1 A brief history of light bending and relativity

We here want to retrace the development of relativistic thought and point out major experiments involving light and especially bending of light trajectories to test general relativity and other theories of gravitation.

Considerations of the gravitational pull of massive objects altering light trajectories go back to Michell, Cavendish, Laplace and Soldner at the turn of the 18^{th} to the 19^{th} century. The first publication to discuss the shift of stellar positions due to Newtonian gravitation was *Über die Ablenkung eines Lichstrahls* ("On the deviation of a light ray") by Soldner [1801]. The effect is noted to be small and to decrease with the separation from the deflecting body. He concluded that considering the state of "practical astronomy" at the time, these effects could be neglected. Indeed experimental results were not obtained until the 20^{th} century.

By that time however, the mechanical worldview had been shaken by the advent of relativity and early quantum mechanics. We shall focus on the evolution of the first which is directly related to the phenomenon of light deflection, studied here.

By the end of the 19^{th} century electromagnetism and mechanics were well established physical theories. They had been in agreement with most experiments, however measurements of the speed of light consistently produced the same value regardless of the velocity of the frame of the laboratory. This is achieved in the famous Michelson–Morley experiment and similar setups. This led Lorentz to propose the transformation, which bears his name and a number of physicists, notably Poincaré to elaborate upon. An elegant solution was proposed in 1905 by an unknown patent clerk named Albert Einstein. His theory which came to fame under the name of the special theory of relativity, solved the kinematic problems of electromagnetism. It was incomplete though, as it did not account for the other fundamental force known at the time, gravitation. The search for a theory capable of explaining and superseding Newtonian mechanics, lead to the geometric theory of gravity called the general theory of relativity.

Over the past century general relativity and its predictions have been tested by a number of solar system experiments. In the subsequent paragraphs, we shall examine a selection of them. Yet let us point out first, that there exist concurrent theories of gravity, some of which are relativistic and do comply with present day experiments in the solar system. general relativity may have the advantage of simplicity, notwithstanding concurrent theories can only be invalidated if their predictions are proven wrong. To make comparisons the parametrized post-Newtonian framework has been developed and we discuss it in section 3.2.3. This will lead us to discuss the reach of the tests feasible with Gaia. It is the challenge of future experiments to reach a precision where deviations from the predictions of general relativity could be detected.

3.1.2 Experimental tests of general relativity

We will present the three classical tests of general relativity and then discuss more recent ones. In the solar system, the predictions of general relativity are in good agreement with Newtonian mechanics and observations. Most planetary orbits are in good agreement with both theories. However there are three instances of physical effects which have helped establish general relativity as a more correct theory than its predecessor. They are: Mercury's perihelion precession, the light deflection by the Sun for grazing rays and gravitational redshift of light. All of them are relatively small effects.

According to Kepler's second law, planet's move on elliptical orbits around the Sun. In Newtonian mechanics, these orbits are perturbed by the small gravitational pull of the other planets. According to Will [1993, p. 4] the three strongest contributions to the rate of precession of Mercury, as predicted by Newtonian theory are due to Venus, the Earth and Jupiter.

After summing the contributions of all planets a discrepancy of $42.7''$ per century remains. The presence of this advance was first noted by Le Verrier in 1859. The value is close to the prediction from general relativity which is $42.95''$ per century.

This effect can be explained heuristically by two contributions. The first is the special relativistic mass increase of the planet. The second is due to the mass associated with the energy density of the Sun's gravitational field. This term adds to the Sun's gravitational potential in the Newtonian picture. This is discussed in further detail in Sexl and Sexl [1979]. Will notes that the solar quadrupole moment may also contribute to this shift. From helioseismic measurements and assumptions about the internal structure of the Sun it has been inferred that its quadrupole moment is $J_2 = (2.2 \pm 0.1)\, 10^{-7}$ [Roxburgh, 2001]. The correction to the precession rate is smaller than experimental errors, hence general relativity passes this test.

The second classical test is the deflection of light by massive objects. Interest in this weak phenomenon was restored by the advent of general relativity. In the solar system the most massive body is the Sun, therefore the deflection due to the Sun was studied first. Notably the 1919 solar eclipse and Eddington's expedition caught public attention. The experiment was performed by two teams in Sobral in Brazil and on the Island of Principe off the Atlantic coast of Africa and measured the displacement of stars close to the Sun. Due to the limitations in optical equipment at the time, observations had to be made during a total eclipse when the Moon blocks out direct Sun light and the field of stars in its vicinity becomes visible. The observations were recorded on photographic plates and compared to records of the same field when the Sun was not present. The results were given as 1.13 ± 0.07 and 0.92 ± 0.17 times the value predicted by Einstein (1.75 arcseconds) [Will, 1993, p. 5]. This value is twice that obtained by Soldner using the Newtonian theory. These results were questioned and indeed offered only weak agreement compared with modern ones. During the 1970's they were finally confirmed with a precision of 1% using radio wave interferometry. A pair of experiments was carried out using a radio interferometer of 35-km base-line at the National Radio Astronomy Observatory (NRAO) in 1974 and 1975. The set up differed also in the angles between the sources and the Sun, nonetheless according to [Fomalont and Sramek, 1976], "the mean gravitational deflection is 1.007 ± 0.009 (standard error) times the value predicted by general relativity". It also gave an estimate of the post-Newtonian parameter $\gamma = 1.014 \pm 0.018$ (standard error) and the corresponding absolute value of deflection at the solar limbs of 1.761 ± 0.016 arcseconds.

This effect has also been employed in the data reduction for Hipparcos and will be for Gaia. The equations describing the phenomenon will be developed later in the parametrized post-Newtonian formalism in section 3.3.5.

The third classical test is gravitational red shift of light. This was the first to be proposed by Einstein himself. Since it is a test of the equivalence principle, we shall discuss it in the sections 3.2.1 and 3.2.2.

Will proposed the time delay of light as a third classical test of general relativity, instead of the red shift experiment for which the predictions of every metric theory of gravitation are identical. In 1964 Irwin Shapiro discovered that a ray of light propagating in the gravitational field of a massive body will traverse a given distance in a longer time, than if the field were absent. In the decades following the discovery of this effect a number of solar system experiments have been carried out. What is measured is the round trip time of a signal emitted from Earth and reflected from another body (planet or space craft). Radar ranging of targets was commonly used. A detailed discussion can be found in Will [1993, p. 173]. It is one of the most precise tests of general relativity. Time delay has also been exploited in the Cassini 2002 Solar Conjunction Experiment which gave the limit $\gamma - 1 \leq 2.3 \cdot 10^{-5}$. This experiment will be discussed in more detail in section 3.2.3.

During the second half of the 20^{th} century, gravitational lensing and gravitational waves emerged as fields of application of general relativity. Both are linked to extragalactic astro-

physics.

The idea that the gravitational bending of light is similar to the action of optical lenses goes back to the earlier years of the theory. It was realised that multiple images of an object can be formed. In 1937 Zwicky predicted gravitational lensing by galaxies and expected the phenomenon to be observable. However the phenomenon was not observed until 1979, when Walsh, Carswell and Weyman detected the first gravitational lens candidate with multiple images. In 1987 Lynds and Petrosian announced "luminous arcs": highly distorted images of high redshift galaxies. Ringlike deformed objects were finally discovered in 1988. An account of the historical evolution of ideas can be found in the introduction of Schneider et al. [1992].

Gravitational waves have been looked for over the past decades, and the sources whose emission if most likely to be picked up are inspiralling close compact systems and mergers of objects like black holes and neutron stars. Recently experimental effort has gone into the development of large scale laser interferometric gravitational-wave observatories on ground such as LIGO in Washington and MiniGRAIL in Leiden (Netherlands) and in space such as the proposed LISA mission. Meanwhile theoretical activity in the field has focused on obtaining accurate predictions of the gravitational wave form signal. There is experimental evidence. Orbital decay due to the emission of gravitational waves has been detected. Its amount is estimated to agree with general relativity to better than half a percent using the Hulse–Taylor binary pulsar, [Weisberg and Taylor, 2005]. Other binary pulsar systems have yielded other tests, especially of strong-field effects. Will [2011] points out that the post-Newtonian approximation, presented in section 3.3.1, has been shown to be "unreasonably effective" for extreme conditions such as mergers of compact objects. When direct observation of gravitational radiation from astrophysical sources begins, new tests of general relativity will be possible.

3.2 Modeling the physics of light propagation

In this section we are concerned with the theoretical framework that allows us to compare contending theories of gravitation. Our goal is the geodesic equation in the parametrized post-Newtonian formalism. This equation will be studied later in simulations using Gaia data.

We will consider the case of metric theories of gravity as defined below. In this case light follows a geodesic line in space-time. Thus the geometry of space-time determines the light path. The distribution of masses determines the geometry (curvature) of space-time, and hence influences light propagation. The effect results in a shift of the apparent position of a star due to the gravitational field along the light path.

The other factor impacting the light path is the theory of gravitation employed, we will see that there are different possible theories of gravitation and present the parametrized post-Newtonian framework which permits a consistent comparative treatment of alternative theories.

In the case of lensing, distortion of the image or even multiple images can occur, we will not go into its details here. In the more modest case of light deflection the light path is only slightly altered and thus the apparent position of stars is changed [Schneider et al., 1992]. We are not concerned with effects such as magnification and distortion of the source, since we will not consider extended sources in our simulations of the astrometric solution for Gaia. For our purposes the deviations will be small enough compared to the apparent size of the objects, to neglect pure lensing effects.

There are different models and formalism to account for gravitational deflection of light. In order to achieve microarcsecond precision in astrometric measurement it is necessary to account for quadrupole light deflection. This is discussed in Klioner [2003]. In Zschocke and Klioner [2011] the tensorial approach for the calculation of light deflection terms, as used in GREM, is outlined. We will follow up on the work by [Crosta and Mignard, 2006] and out forward a simplified relativistic model accounting for quadrupole light deflection in the source direction calculation of AGISLab. There is also a dipolar light deflection effect due

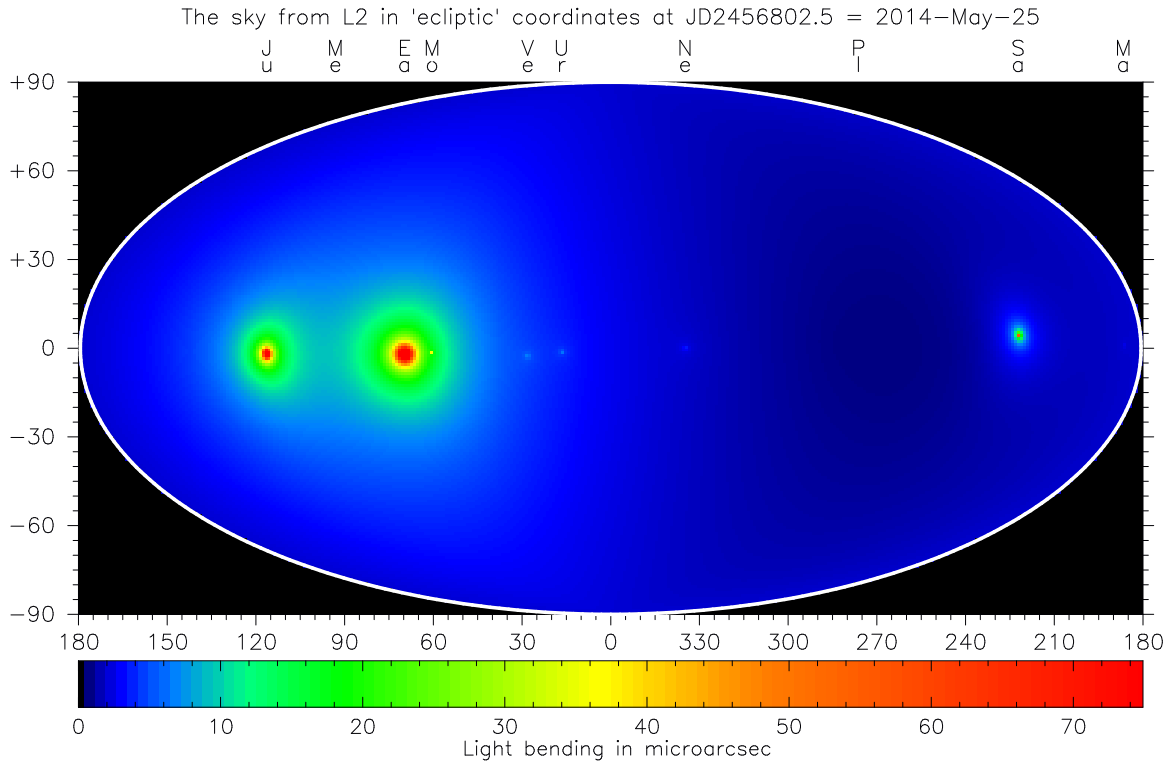

Figure 10: This map of the sky shows the total post-Newtonian light deflection due to all planets, and the Moon, at 25 May 2014. This representation uses ecliptic coordinates, for an L2-based observer. The contribution from the Sun has been suppressed because it is immense compared to the other bodies and extends all over the sky. The colour coding shows significant light bending is predicted in regions coloured different from blue. Two-letter object-name abbreviations, above the top axis, label the deflecting objects. (Credit : Jos de Bruijne ESA Science Team [2010], Gaia: Gravitational Light Deflection)

to the motion of the planets. This has been discussed by Kopeikin and Makarov [2007]. It will not be further investigated here. We believe that the model presented here will be less computationally intensive than the full GREM and that the comparison of results will be valuable.

3.2.1 Relativity principles

The principle of equivalence was already stated by Newton in his *Philosophiae Naturalis Principia Mathematica* (1687). As noted by [Will, 1993] Newton's principle can be stated as the "inertial mass" of a body is equal to its "passive gravitational mass". Today this is called the *Weak Equivalence Principle* (WEP). In modern terms as stated by [Will, 1993] (p.22) it is :

> "*If an uncharged test body is placed at an initial event in spacetime and given an initial velocity there, then its subsequent trajectory will be independent of its internal structure and composition.*"

Where "uncharged" refers to the object having zero electrical charge. The "test body" is required to have negligible self-gravitational energy and has to be small enough so that coupling to external inhomogeneities can be ignored. This idea lies at the foundations of relativity. In this section we discuss different versions of the equivalence principle and their relation to theories of gravitation.

A local nongravitational test experiment has to comply with the following requirements:

(i) *be performed in a freely falling laboratory that is shielded and is sufficiently small that inhomogeneities in the external fields can be ignored*,

(ii) *in which self-gravitational effects are negligible.*

Based on the two preceding defintions, the Einsteinian Equivalence Principle (EEP) is formulated in the following way by Will :

(i) *The Weak Equivalence Principle is valid,*

(ii) *The outcome of any local nongravitational test experiment is independent of the velocity of the (freely falling) apparatus,*

(iii) *The outcome of any local nongravitational test experiment is independent of where and when in the Universe it is performed.*

The theories we will discuss later will satisfy the postulates of Metric Theories of Gravity, as formulated by Will:

(i) *Spacetime is endowed with a metric tensor g,*

(ii) *The world lines of test bodies are geodesics of that metric,*

(iii) *In local free falling frames, called Lorentz frames, the nongravitational laws of physics are those of special relativity.*

As Will has pointed out, a theory satisfying EEP would appear to satisfy these postulates of Metric Theories of Gravity. Examples of metric theories of gravity are general relativity, the Rosen bimetric theory and Brans-Dicke theory and the theory of general relativity which are discussed in Will [1993].

EEP entails that all nongravitational laws of physics must be Lorentz invariant, this is called Local Lorentz Invariance. This is the second requirement of EEP. The postulate of Local Position Invariance says that "the results of local nongravitational test experiments must be independent of the spacetime location of the frame". It is in fact the third requirement of EEP.

The strong equivalence principle (SEP) states that:

(i) *WEP is valid for self-gravitating bodies as well as for test bodies,*

(ii) *The outcome of any local test experiment is independent of the velocity of the (freely falling) apparatus,*

(iii) *The outcome of any local test experiment is independent of where and when in the Universe it is performed.*

The difference between EEP and SEP, is that the latter includes self gravitating bodies as well as experiments involving gravitational forces such as Cavendish experiments and gravimeter measurements. However EEP is included in SEP in the case where the local gravitational forces can be ignored. Will notes that it can be deduced from SEP that there "*there must be one and only one gravitational field in the universe, the metric g*". general relativity respects SEP.

To close this discussion on the principles of relativity, it seems appropriate to consider the connection between WEP and EEP. Leonard I. Schiff conjectured that in fact (we quote the formulation used by [Will, 1993]): "any complete self-consistent theory of gravity that embodies WEP necessarily embodies EEP." If Schiff's conjecture is correct WEP guarantees Local Lorentz Invariance and Local Position Invariance.

The first successful attempt to prove Schiff's conjecture more formally was made by Lightman and Lee [1973]. They developed a framework called the TH$\varepsilon\mu$ formalism that encompasses all metric theories of gravity and many non-metric theories. They show that if one considers electromagnetic interactions only, the rate of fall of a "test" body made up of interacting

charged particles is independent of the internal electromagnetic structure of the body. Which shows that, given their restrictions, WEP implies EEP.

According to Will [2006, section 2.3], there is mounting theoretical evidence to suggest that EEP is likely to be violated at some level, whether by quantum gravity effects, by effects arising from string theory, or by hitherto undetected interactions. "In string theory, for instance, the existence of EEP-violating fields is assured, but the theory is not yet mature enough to enable a robust calculation of their strength relative to gravity, or a determination of whether they are long range, like gravity, or short range, like the nuclear and weak interactions, and thus too short range to be detectable."

Despite the possible existence of long-range gravitational fields in addition to the metric in various metric theories of gravity, the postulates of those theories demand that matter and non-gravitational fields be completely oblivious to them. The only gravitational field that enters the equations of motion is the metric g. The role of the other fields that a theory may contain can only be that of helping to generate the spacetime curvature associated with the metric. Matter may create these fields. These fields together with the matter density may generate the metric, but they cannot act back directly on the matter. Matter responds only to the metric. [Will, 2006]

3.2.2 Tests of the equivalence principle

Since the equivalence principle lays the foundation for general relativity, a number of experiments to test its validity have been devised. In the following we shall discuss the Eötvös experiment and the gravitational red shift of light.

To test the equivalence principle one looks for variations in the effects of physical laws for bodies of different composition. Supposing that the inertial mass and passive gravitational mass of an object are different, one can define a quantity called "Eötvös ratio" usually denoted η. Using two bodies of different composition, for instance one made of iron and another made of carbon, one can measure the corresponding "Eötvös ratio". This can be carried out by using a pendulum or the classic torsion balance used by Eötvös. Recently a sophisticated torsion balance tray has been used for the "Eöt–Wash" experiments carried out at the University of Washington, to compare the accelerations of various materials toward local topography on Earth, movable laboratory masses, the Sun and the galaxy. These tests have reached a level of $3 \cdot 10^{-13}$. [Adelberger [2001], Baeßler et al. [1999], Su et al. [1994] as cited by Will [2006].] Therefore WEP is well supported by the Eötvös experiment. Possible space bound tests of WEP are STEP and MICROSCOPE [Will, 2006].

Let us come back now to the third classical test of general relativity, the gravitational red shift of light, which was predicted by Einstein in 1911. Since it is a test of the equivalence principle, all metric theories of gravity predict the same value. A typical gravitational redshift experiment measures the frequency or wavelength shift $Z = \Delta\nu/\nu = \Delta\lambda/\lambda$ between two identical frequency standards (clocks) placed at rest at different heights in a static gravitational field. The comparison of their frequencies is directly related to the comparison of the velocities of two local Lorentz frames. Measuring it was challenging, the first successful redshift measurment were the Pound–Rebka–Snider experiments of 1960 to 1965. They measured the frequency shift of gamma-ray photons emitted from ^{57}Fe as they ascended or descended the Jefferson Physical Laboratory tower. There were attempts to use solar spectral lines for redshift experiments, but solar spectral lines are strongly affected by the Doppler shift, only in 1962 a realisable experiment was made.

3.2.3 The parametrized post-Newtonian formalism

As early as 1922 Sir Arthur Stanley Eddington had parametrized the post-Newtonian approximation, to work with the vacuum gravitational field exterior to an isolated spherical body. A modern version of the PPN formalism was pioneered by Kenneth Nordtvedt, who studied the post-Newtonian metric of a system of gravitating point masses, extending earlier work by Eddington, Robertson and Schiff [Will, 1993, section 4.2]. The generalization of the framework to include perfect fluids was elaborated by Will. Together, Will and Nordtvedt developed a general and unified version of the PPN formalism. Other versions of the PPN formalism have been developed to deal with point masses with charge, fluid with anisotropic stresses, bodies with strong internal gravity, and post-post-Newtonian effects [Will, 1993, section 4.2 and 14.2].

The formalism was devised to allow comparison between different theories of gravitation and experiments. It is in the words of Will a "theory of theories of gravity". The motivation for the development of this framework was the advent of alternative theories of gravity during the second half of the 20^{th} century which, although they are based on the equivalence principle, make predictions that differ from those of general relativity. A range of alternative theories have been mentioned in 3.2.1, of which a detailed discussion can be found in chapter 5 of Will [1993] and in section 3.3 of Will [2006].

This framework is an important tool for the comparison of different metric theories of gravity and has been applied in the analysis of solar system gravitational experiments. It has provided a means to quantify the possible deviation from general relativity, which as we shall see is small for all effects of post-Newtonian order.

The comparison of competing theories of gravity necessitates a coherent presentation in terms of mathematical notation. This notation covers the coordinates, the matter variables, the metric tensor of the theory as well as other scalar, vector and tensor fields involved in the theory. Because the metric and the equations of motion for matter are the predominant entities for calculating observable effects, what distinguishes one metric theory from another is the specific mechanism through which matter and possibly other gravitational fields generate the metric. Rigorous definitions and detailed calculations of these can be found in Will [1993].

Will [1993] shows that the comparison of metric theories of gravity with each other and with experiment becomes particularly simple when one takes the slow-motion, weak-field limit. This approximation is known as the post-Newtonian limit, discussed in 3.3.1. According to Will, it is sufficiently accurate to encompass most solar-system tests that can be performed in the foreseeable future. In this limit, the spacetime metric g predicted by nearly every metric theory of gravity has the same structure. It can be written as an expansion about the Minkowski metric ($\eta_{\mu\nu} = \text{diag}(-1, 1, 1, 1)$) in terms of dimensionless gravitational potentials of varying degrees of smallness. These potentials are constructed from the matter variables by analogy of the Newtonian gravitational potential.

In the parametrized post-Newtonian framework there are ten parameters which describe the behaviour of a theory of gravitation in the post-Newtonian limit. They are dimensionless quantities, but do correspond to physical effects depending on the post-Newtonian potential they are associated with. The complete set of parameters with their values in general relativity and two other classes of theories are shown in table 2.

Will uses the terms "fully conservative theory" and "semi-conservative theory" to express the conservation laws the theories possess .

A "fully conservative theory" is any theory of gravitation which possesses the conservation laws of total momentum (i.e. energy and momentum), angular momentum and center of mass motion. That is, all of the post-Newtonian conservation laws hold. It can be shown that for such a theory the post-Newtonian limit has three free PPM parameters γ, β, ξ. In particular, such theories do not predict any post-Newtonian preferred-frame effects.

A "semi-conservative theory" is any theory of gravitation which possesses the conservation laws of total momentum. Any theory that is based on an invariant action principle is semi-

conservative and has five free PPN parameters $\gamma, \beta, \xi, \alpha_1, \alpha_2$. The effects associated with the

Parameter	What it measures relative to GR	Value in GR	Value in semi-conservative theories	Value in fully conservative theories
γ	How much space-curvature produced by unit rest mass?	1	γ	γ
β	How much "nonlinearity" in the superposition law for gravity?	1	β	β
ξ	Preferred-location effects?	0	ξ	ξ
α_1	Preferred-frame effects?	0	α_1	0
α_2		0	α_2	0
α_3		0	0	0
α_3	Violation of conservation	0	0	0
ζ_1	of total momentum?	0	0	0
ζ_2		0	0	0
ζ_3		0	0	0
ζ_4		0	0	0

Table 1: The PPN Parameters and their significance (note that α_3 is shown twice to indicate that it is a measure of two effects), from Will [2006, table 2 p. 29]

parameters can be tested by different kinds of experiments which we shall discuss briefly.

The "preferred frame" and "preferred location" effects are violations of SEP predicted by certain theories of gravity. They indicated that outcomes of local gravitational experiments may depend on special properties of the location or the frame in which they are carried out. For "preferred frame" effects, which are accounted for by the α_i parameters, this means that the outcome may depend on the velocity of the laboratory relative to mean rest frame of the universe. The Lense–Thirring effect or "dragging of inertial frames" is a gravitomagnetic effect in the sense that it describes a contribution to the gravitational field originating from the motion or rotation of matter. This effect is predicted by general relativity and involves γ and α_1. It has been tested by the Relativity Gyroscope Experiment (Gravity Probe B).

In the case of "preferred location" effects the outcome may depend on the location of the laboratory relative to a nearby gravitating body. The latter are accounted for in the ξ parameter. To give but one example let us mention the so-called "Whitehead" effects, referring to galaxy-induced anisotropy in the local gravitational constant G_L.

The five parameters $\zeta_1, \zeta_2, \zeta_3, \zeta_4$ and α_3 are associated with the conservation laws of total momentum. ζ_4 is associated with the gravity generated by fluid pressure and for theoretical reasons (see Will [2006] p.48) it follows that $6\zeta_4 = 3\alpha_3 + 2\zeta_1 - 3\zeta_3$. This is the equation that table 2 is referring to as equation (58). According to Will [2006, section 3.7.3] a non zero value of any of those parameters would entail a violation the conservation of momentum, or equivalently of the equality of action and reaction in the Newtonian limit.

The Eddington–Robertson–Schiff parameters γ and β are used to describe the "classical" tests of GR. In a sense they are the most important; they are the only non-zero parameters in GR and scalar-tensor gravity.

The β parameter measures the non-linearity in the superposition law of gravity. That is whether gravitational fields do interact with each other. Its value in general relativity is one. To conclude this section it is of interest to point out that there are a variety of other effects

which may involve any number of PPN parameters, let us just mention that when including PPN contributions to the perihelion shift of Mercury, β is involved along with $\gamma, \alpha_1, \alpha_2, \alpha_3$ and ζ_2. Another class of experiments that allow us to determine β are measurements of the Norvedt effect. Norvedt showed [Nordtvedt Jr, 1968] that a number metric theories of gravity predict violations of the Weak Equivalence Principle for massive bodies. More precisely their acceleration will depend on their gravitational self energy. The formula as given in Will [2006] reads :

$$\mathbf{a} = \frac{m}{m_p}\nabla U = \left(1 - \eta_N \frac{E_g}{m}\right)\nabla U \tag{2}$$

$$\eta_N = 4\beta - \gamma - 3 - 10\xi/3 - \alpha_1 + 2\alpha_2/3 - 2\zeta_1/3 - \zeta_2/3 \tag{3}$$

Asteroid tracking with Gaia will provide new bounds on β. Indeed asteroids are very common objects in the solar system and can be found on elliptical orbits of high eccentricity. Although they are faint for Solar System objects, many of them can be detected by Gaia. They have the advantage of having little mass and behaving very closely like test particles. Gaia's high precision astrometry will permit us to measure the perihelion shift of these objects, at different distances from the Sun, and thus permit to discern between the contributions of β and the Solar quadrupole moment J_2. However, non-gravitational interactions, such as collisions, may produce perturbations to the predicted effects. This is discussed in [Hestroffer et al., 2010], they expect a precision with standard deviations of about $0.6 < \sigma_\beta \cdot 10^4 < 6$ and $0.5 < \sigma_{J_2} \cdot 10^8 < 10$.

The γ parameter is of great interest for the present work since its precise determination is possible using Gaia data and is necessary to produce a star catalog of μarcsec precision. It quantifies the space-curvature produced by unit rest mass. Its value in general relativity is one. Therefore it appears in effects and measurements which probe this curvature, such as light bending and time delay of light. According to Bertotti et al. [2003], "the quantity $(\gamma - 1)$ measures the degree to which gravity is not a purely geometric effect and is affected by other fields ; such fields may have strongly influenced the early Universe, but would have now weakened so as to produce tiny – but still detectable – effects". It is also related to the precession of a gyroscope in curved space time. In sections 3.3.2 and 3.3.5 we will see that PPN γ appears in the formula for the light deflection angle.

The Cassini 2002 Solar Conjunction Experiment constitutes the most precise measurement of PPN γ to-date. Bertotti et al. [2003] report a measurement of the frequency shift of radio photons to and from the Cassini spacecraft as they passed close to the Sun. They found $\gamma = 1 + (2.1 \pm 2.3) \cdot 10^{-5}$. This can be compared to the precision of previous astrometric observations, Froeschle et al. [1997] have calculated an estimate of PPN γ from Hipparcos data. Their final result is $\gamma = 0.997 \pm 0.003$, which is about two orders of magnitude worse. Gaia is expected to give an accuracy of up to 10^{-6} [Hobbs et al., 2010].

Over the past decades, experiments of increasing precision have been carried out. The bounds which were obtained are shown in Table 2. It has been shown that the values of the parameters are close to those they take in general relativity. The maximal deviation is 2% for ζ_1 which has not been measured directly but was deduced from combined bounds on the PPN parameters. The best known parameter is α_3 whichhas been inferred from measurements of the time derivatives of pulsar periods. [Will, 2006, p.46].

To test the precision to which general relativity fits the solar system dynamics and improve the bounds on the PPN parameters new missions have been proposed. Aside from Gaia which we have already discussed, there are a number of other interesting experiments. The Laser Astrometric Test Of Relativity (LATOR) is a proposed NASA mission that will attempt to improve the precision of γ by light deflection measurements, the quadrupole moment of the sun J_2, and the solar frame-dragging effect, using optical tracking and an optical interferometry on the International Space Station. It may also measure effects of the next post-Newtonian order (c^{-4}) of light deflection resulting from the non-linearity in gravitation. The Apache

Parameter	Effect	Limit	Remarks
$\gamma - 1$	time delay	2.3×10^{-5}	Cassini tracking
	light deflection	4×10^{-4}	VLBI
$\beta - 1$	perihelion shift	3×10^{-3}	$J_2 = 10^{-7}$ from helioseismology
	Nordtvedt effect	2.3×10^{-4}	$\eta_{\mathrm{N}} = 4\beta - \gamma - 3$ assumed
ξ	Earth tides	10^{-3}	gravimeter data
α_1	orbital polarization	10^{-4}	Lunar laser ranging
		2×10^{-4}	PSR J2317+1439
α_2	spin precession	4×10^{-7}	solar alignment with ecliptic
α_3	pulsar acceleration	4×10^{-20}	pulsar $\dot{P}$ statistics
η_{N}	Nordtvedt effect	9×10^{-4}	lunar laser ranging
ζ_1	—	2×10^{-2}	combined PPN bounds
ζ_2	binary acceleration	4×10^{-5}	$\ddot{P}_{\mathrm{p}}$ for PSR 1913+16
ζ_3	Newton's 3rd law	10^{-8}	lunar acceleration
ζ_4	—	—	not independent (see Equation (58))

Table 2: Current limits on the PPN parameters. Here η_N is a combination of other parameters given by eq. (3), from Will [2006, table 4 p.43]

Point Observatory Lunar Laser-ranging Operation is the successor of the Lunar Laser Ranging experiment which established bounds on β. The proposed proposed ESA Bepi-Columbo Mercury orbiter would also improve the understanding of possible variations of the Gravitational constant and the parameters γ, β, α_1 and J_2. As mentioned by Will [2006], Nordtvedt has argued that "grand fits" of large solar system ranging data sets, including radar ranging to Mercury, Mars, and satellites, and laser ranging to the Moon, could yield substantially improved measurements of PPN parameters.

3.2.4 Coordinate systems and relativity

Coordinates are needed to process Gaia data. For convenience different coordinate systems are in use, this is partly due to the motion of the spacecraft and observers with respect to the rest of the universe. In this section we discuss the astronomical reference systems used for Gaia and the distinction from the mechanical reference systems used to describe the satellite.

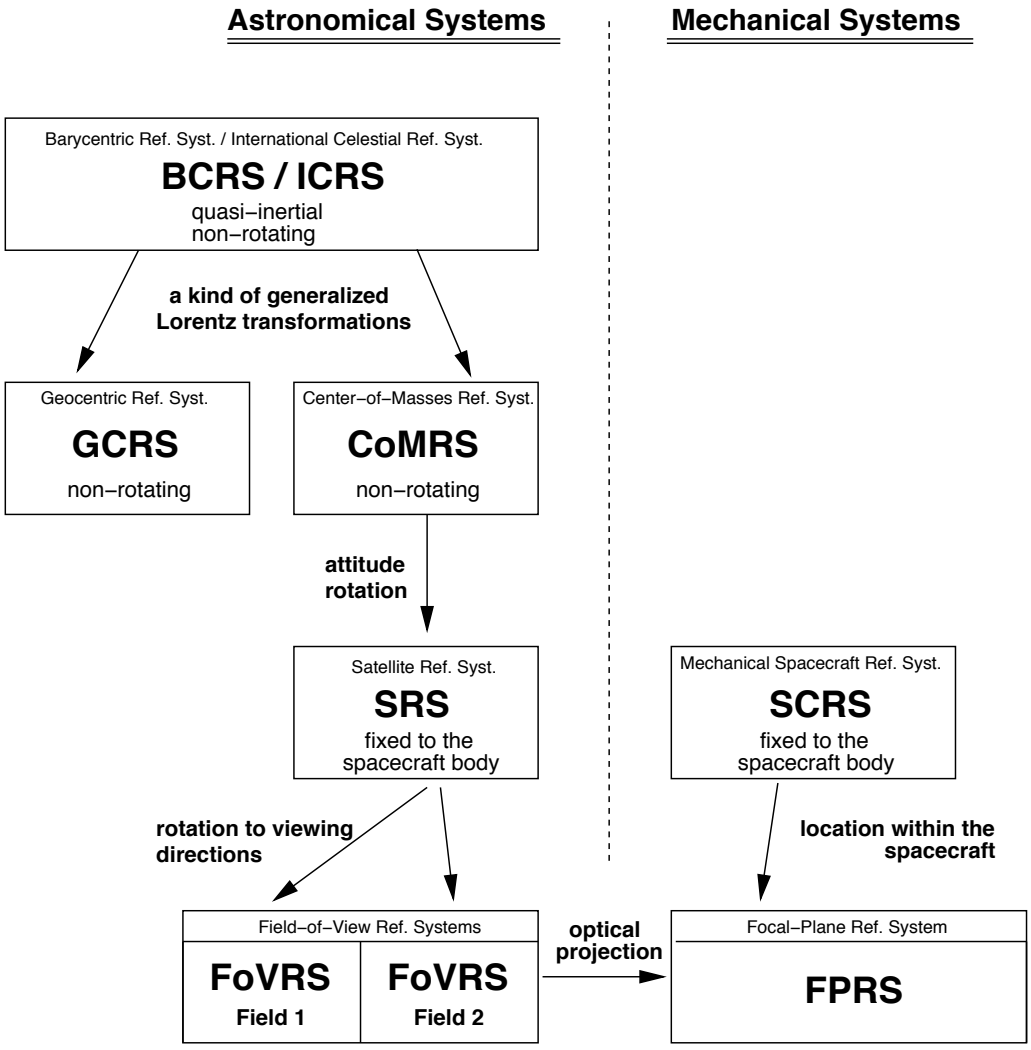

Figure 11: Overview of the reference systems associated with Gaia (BCRS, CoMRS, SRS) discussed below from [Bastian, 2007, Chapter 4].

Reference systems and reference frames As explained by [Bastian, 2007] there is a distinction between reference systems and reference frames.

1. A *reference system* gives an idealised, abstract definition of a coordinate system.

2. A *reference frame* is a practical realisation of such a system.

The astronomical reference systems used here are the ICRS and derivatives of it (e.g. BCRS). In the following we outline the definitions of ICRS/BCRS, CoMRS and SRS. These reference systems must be fully relativistic to comply with the precision goals of Gaia. We will explain how transformations between them are take into account in data processing and in

AGISLab. An overview of the different reference systems used in the context of Gaia is given in figure 11.

According to [Bastian, 2007], the International Celestial Reference System (ICRS) and the Barycentric Reference System (BCRS) are defined as a quasi-inertial and rotation-free reference system. The BCRS is defined to be nonrotating with respect to distant extragalactic objects, its origin is the solar-system barycentre. A precise definition as given by the IAU convention can be found in Rickman [2001].

The ICRF is the primary reference for astronomical coordinates, its realisation is the International Celestial Reference Frame (ICRF). The position of stars, or more generally, directions (toward stars) in the astronomical sense, are given in the International Celestial Reference System (ICRS). The Barycentric Coordinate Time (TCB) is the basic time coordinate for all Gaia data processing. The spatial orientation of the ICRF is defined by a set of distant radio sources observed with the VLBI. A secondary realisation is the Hipparcos Catalogue. A realisation of the ICRF must also provide an ephemeris giving the three-dimensional spatial coordinates of solar-system bodies as function of a time coordinate. The coordinates used for the Gaia mission and AGIS are equatorial coordinates $(\alpha, \delta, \dots)$, they are discussed in the paragraph on coordinate systems below. The time coordinate is also discussed below There are two main practical realisations, one is the "Development Ephemeris" series provided by by the JPL (Pasadena) and the other are the ephemerides of IMCCE (Paris). The ICRF as a practical realisation of the ICRS may be imperfect. Rotational and translational non-inertiality of the frame can be due to the uncertainties in the experimentally measurable quantities (angles, precession rates etc.). A summary of the complete post-Newtonian metric and other formulae in the ICRS can be found in Soffel et al. [2003].

In [Bastian, 2007] it is pointed out that: "Ecliptic and galactic coordinates are alternate coordinates for the ICRS". As such they are not distinct reference systems, however for interpretation of results of the Gaia mission it is convenient to use transformations from the equatorial ICRS coordinates to these coordinate systems. Bastian mentions that there is a 10-digit version of these transformations given in the Hipparcos catalog.

The Center-of-Mass Reference System of Gaia (CoMRS) has its spatial origin at the center of mass of the Gaia satellite. It must be defined fully relativistically. Per definition it is supposed to be kinematically non-rotating with respect to the ICRS/BCRS. The definition of the CoMRS and a discussion is given in from Bastian [2007, section 4.2.3] and references therein. The transformations from BCRS to CoMRS are a central part of the relativity modeling for Gaia and are studied by the REMAT group. A concise and useful description is given in Lindegren [2001] and the definitions are given in Klioner [2004].

The Scanning Reference System (SRS) is co-moving and co-rotating with the body of the Gaia spacecraft. It is rigidly connected to the body of the Gaia spacecraft (which in turn is assumed to be a rigid body) and its origin is at the center of mass of Gaia. Therefore the transformation from CoMRS to SRS is the attitude rotation. This is illustrated in figure 4 (a). The main use of the SRS is to define the satellite attitude. The natural time coordinate is the proper time of the spacecraft. The practical realisation of the SRS consists mainly of a model for the attitude as function of time. According to Bastian [2007] there are several such models: the nominal attitude (sometimes also called nominal scanning law), the real-time attitude, (also called on-board attitude), the high-precision scientific attitude, reconstructed on ground from the measurements performed by the Gaia instruments. The latter will be an approximation of the real attitude at the level of 10μarcsec.

The relations between different reference frames are illustrated in figure 11. BCRS and CoMRS are connected by a generalized Lorentz transformation in a similar fashion as BCRS is connected to the Geocentric Reference System (GCRS) [which is defined in the IAU Resolution B1.3 (2000)].

Coordinate systems The 'world line' of a physical body is given by three spatial coordinates and a time coordinate. In astronomy the sky is usually mapped by a spherical coordinate system, two angles describing an object's direction in the sky and the third coordinate being the distance to the origin, its parallax. By convention, the angular coordinates are called right ascension α and declination δ . They are the spherical longitude and latitude respectively and represent the coordinate direction of the body.

In BCRS the unit vectors along the principal directions are denoted $\mathbf{X}, \mathbf{Y}, \mathbf{Z}$. Where $\mathbf{X}$ points towards $(\alpha, \delta) = (0, 0)$, $\mathbf{Z}$ points towards the ICRS north pole ($\delta = +90°$),and $\mathbf{Y} = \mathbf{Z} \times \mathbf{X}$. They form a right-handed coordinate system. A general unit vector $\mathbf{u}$ has direction cosines X, Y, Z, such that $X^2 + Y^2 + Z^2 = 1$:

$$\mathbf{u} = X\mathbf{X} + Y\mathbf{Y} + Z\mathbf{Z} = \cos(\alpha)\cos(\delta)\mathbf{X} + \sin(\alpha)\cos(\delta)\mathbf{Y} + \sin(\delta)\mathbf{Z} \tag{4}$$

Bastian [2007] further points out that there is no physical unit associated with the cartesian coordinates (X, Y, Z). The coordinate system is illustrated in figure 4 (b).

The Barycentric Coordinate Time (TCB) is the natural time coordinate used with ICRS. The transformations to other relevant time coordinates, such as TT, TAI and UTC [7] , are non trivial and must account for relativistic effects and orbital motions. Bastian notes that "the precision of these transformations increases with time due to better ephemerides and general physical knowledge". The proper motions associated with (α, δ) are denoted $\mu_\alpha = \partial_t \alpha = \dot{\alpha}$ and $\mu_\delta = \partial_t \delta = \dot{\delta}$. Using the TCB time coordinate for the time derivative.

A star (source) is described by its direction, parallax, proper motion, radial velocity and magnitude. The proper motion of a star is the change in its position over time with respect to the barycenter of the Solar System [Kovalevsky, 2002]. The radial velocity is particularly hard to measure and its determination relies on the spectroscopic instrument. It will not be solved for by AGIS accurately and high precision follow up measurements will be needed [Jasniewicz et al., 2011].

Time Coordinate The different physical time scales used for Gaia are to be considered in a relativistic context. These different time scales are a result of time dilation of moving objects, as predicted by special relativity, and the general-relativistic time dilation of objects in a gravitational potential, as predicted by general relativity. [Bastian, 2007]

As mentioned above the natural time coordinate in ICRS is TCB, it will be used for Gaia data processing. The Barycentric Coordinate Time (TCB) is the time-like coordinate of the Barycentric Reference System (BCRS). In the data processing, this time coordinate will be used in its representation in terms of nanoseconds since J2010.0 (TCB) [8] In the Java toolbox "GaiaTools", the two fundamental Java classes "GaiaTime" and "EarthTime" encapsulate the useful representations and transformations. [Bastian, 2007]

[7] These are according to Bastian [2007]: Terrestrial Time (TT) is approximately the time of a clock on the geoid, International Atomic Time (TAI) is the practical realisation of TT Coordinated Universal Time : UTC = TAI + leap seconds, Geocentric Coordinate Time (TCG), T_G the proper time of Gaia's master clock and its realisation On-board Time (OBT).

[8] This uses the Julian year, defined in Bastian [2007].

3.3 Equations for light propagation in the post-Newtonian limit

The pivotal point in astrometry is stressed by [Bastian, 2007](section 4.2.1.3, p. 22):

> *The primary quantity to be measured is the direction of light rays. This quantity also can be expressed in the ICRS by spherical longitude and latitude coordinates (α) and (δ), or else by Cartesian unit vectors. Conceptually, however, it should not be mixed up with the BCRS coordinates of the corresponding body from which the light ray originated. Light rays are curved, and the observed direction of a light ray depends on the point of observation and on the motion of the observer.*

This sums up two essential features in relativistic astrometry: that the geometry of space has to be taken into account and that the motion of the observer has to be accounted for. Both are crucial to making the best use of Gaia data.

What is needed to achieve this is a metric theory of gravity and a set of frames, coordinates and data about the physical universe (mass distributions) to provide a model for light propagation. Several different approaches to this problem exist and have been outlined in Klioner [2003], Crosta and Mignard [2006], Kopeikin and Makarov [2007] and Crosta [2010]. In this study of light deflection by Jupiter we have followed the model presented in Crosta and Mignard [2006] and implemented it for calculations in AGISLab.

In this section, we will present the main results of the post-Newtonian approximation useful in our calculation. Here PPN γ will make its appearance to quantify the possible deviations of physical universe from general relativity. We then present the model used for the planet (multipole expansion) and then the equations derived in Crosta and Mignard [2006] as well as the derivation of a quantity needed for calculations in AGISLab.

3.3.1 The post-Newtonian limit for theories of gravitation

We outline how the post-Newtonian Limit of a gravitational theory is obtained. [Will, 1993] gives a detailed overview covering the procedure for different kinds of theories in chapter 5. We will discuss the main steps and then go on to the post-Newtonian equations of light bending we study here.

The field equations of general relativity : (5) are elegant and deceptively simple, showing how geometry is generated by matter.

$$G_{\mu\nu} = \frac{8\pi G}{c^4} T_{\mu\nu} \tag{5}$$

$$\left(-\partial^2_{ct} + \nabla^2 \right) h^{\alpha\beta} = -\frac{16\pi G}{c^4} \tau^{\alpha\beta} \tag{6}$$

Where $G_{\mu\nu}$ is the Einstein tensor which is a function of the components of the metric ($g_{\alpha\beta}$), its first derivatives and its second derivatives. For a given material energy-momentum tensor $T_{\mu\nu}$, (5) are second order differential equations constraining the metric, and thereby defining the geometry of space-time. [9] The constant G is Newton's constant of gravitation and c is the speed of light in vacuum, their units are discussed in appendix C. The quantity $8\pi G/c^4 = 2.07 * 10^{-43}[\mathrm{s}^2\mathrm{m}^{-1}\mathrm{kg}^{-1}]$ is called Einstein's constant of gravitation.

The space-time metric being $g_{\alpha\beta}$ and $g = \det(g_{\alpha\beta})$. The tensor $h_{\alpha\beta}$ in (6) is used in the post-Newtonian approximation. It quantifies the deviation of the metric from the flat Minkowski metric which is ($\eta_{\alpha\beta}$):

$$h^{\alpha\beta} = \eta^{\alpha\beta} - (-g)^{1/2} g^{\alpha\beta}. \tag{7}$$

The "relaxed" Einstein equations (6) are employed in post-Newtonian calculations. Will in Will [2011] calls $\tau^{\alpha\beta}$ the "effective" energy-momentum pseudotensor. It can be directly seen that (6) are a second order differential equations.

[9] The Einstein tensor is a function of the Riemann curvature tensor. Definitions are given in appendix B.

The post-Newtonian approximation supposes that gravitational fields are weak and that characteristic motions of matter are slow compared to the speed of light. As pointed out by Will [2011], this means that for the system in question the quantity $\varepsilon \sim (v/c)^2 \sim GM/(Rc^2) \rightsquigarrow 0$ is small. Here v, M, R denote the characteristic velocity, mass, and distance within the system. He stresses that it is unkown whether the post-Newtonian expansion forms a convergent series.

In brief the steps to calculate the post-Newtonian limit of a metric theory of gravitation according to [Will, 1993](chapter 5) are shown in table 3.

step 1:	identify the variables of the theory
step 2:	set cosmological boundary conditions
step 3:	expand in a post-Newtonian series about asymptotic values
step 4:	substitute into field equations
step 5:	solve for the metric element h_{00} to second order
step 6:	solve for the metric elements h_{ij} to second order and solve for h_{0j} to third order
step 7:	solve for the metric elements h_{00} to fourth order. (Will mentions that this is the biggest step and involves the non-linearities of the theory.)
step 8:	convert to local quasi-cartesian coordinates and standard PPN gauge
step 9:	comparison with a reference "shape" of the equations to read of the values of the parameters

Table 3: Procedure to deduce the post-Newtonian limit of a metric theory of gravitation according to [Will, 1993](chapter 5).

The values of the PPN parameters for general relativity, as given in table 1, are:

$$\begin{aligned} \gamma \;=\; \beta \;&= 1 \\ \xi \;&= 0 \\ \alpha_1 = \alpha_2 = \alpha_3 \;&= 0 \\ \zeta_1 = \zeta_2 = \zeta_3 = \zeta_4 \;&= 0 \end{aligned}$$

We note that general relativity is a fully conservative theory, as a consequence of $\alpha_i = 0$ and $\zeta_i = 0$, without preferred frame effects ($\alpha_i = 0$). For alternative theories these parameters will depend on its fundamental scalar and vector fields.

3.3.2 Equations of light propagation

Our goal is to compare the difference in light deflection effects predicted by alternative theories of gravitation in the post-Newtonian limit. This case is relevant for observations of light deflection by the giant planets of the solar system with Gaia. We denote the coordinates x^β, with Greek indices ranging form 0 to 3.

In the limit of geometrical optics, that is when the wave length of the electromagnetic wave of our light ray is small compared with the scale at which its amplitude changes and the scale at which the background geometry changes, we have along the light path:

$$g_{\alpha\beta}\partial_\lambda x^\alpha \partial_\lambda x^\beta \;=\; 0 \tag{8}$$

$$\partial_\lambda x^\alpha \left(\partial_\lambda x^\beta\right)_{;\alpha} \;=\; 0 \tag{9}$$

This is the geodetic equation for a light ray. As discussed in Will [1993, equation (6.7)],where λ is the "affine" parameter measuring the length along the light path. $A_{;\alpha}$ denotes the covariant derivative of A. The first relation (8) shows that the trajectory of the light ray is a null-geodesic. The equation (9) leads to (10), where Gamma is the Christoffel symbol:

$$\partial^2_\lambda x^\mu + \Gamma^\mu_{\alpha\beta}\partial_\lambda x^\alpha \partial_\lambda x^\beta \;=\; 0 \tag{10}$$

From which one can deduce, by applying the post-Newtonian approximation and the parametrized post-Newtonian framework:

$$\frac{d^2x^j}{dt^2} = \partial_j U \left(1 + \gamma\, \delta_{ik} \frac{dx^i}{dt}\frac{dx^k}{dt} \right) - 2(1+\gamma) \frac{dx^j}{dt} \left(\delta_{ik} \frac{dx^i}{dt}\, \partial_k U \right) \tag{11}$$

Where U is an arbitrary gravitational potential satisfying conditions discussed in the next section (3.3.3) and δ_{ij} is the Kronecker delta. This is expression (1) used by Crosta and Mignard [2006].

3.3.3 The multipole expansion

In this section we discuss the gravitational potential we use. This is part of the modeling of the light deflection problem as discussed above. A potential is needed for equation (22). The shape of the potential determines the effects which can be obtained from it. The expression, valid in any coordinate system, for the gravitational potential of a given mass distribution described by a density ρ is :

$$U(\mathbf{x}, t) = \int_B d^3r\, \frac{G\rho(\mathbf{r}, t)}{||\mathbf{x} - \mathbf{r}||} \tag{12}$$

where $\mathbf{x} = (x^1, x^2, x^3)$ is the coordinate three vector of the point at which we compute the potential, $\mathbf{r}$ is the coordinate three vector of integration and B designates the volume occupied by the mass distribution, which may depend on time. The density ρ measures the rest-mass density in a local freely falling frame momentarily comoving with the gravitating matter.

Since our objective is to calculate the gravitational potential of a giant gaseous planet the multipole expansion is a useful tool in simplifying expression (12). It is obtained by Taylor expansion of the norm $||\mathbf{x} - \mathbf{r}||$:

$$\frac{1}{||\mathbf{x} - \mathbf{r}||} = \left(\mathbf{x}^2 - 2\mathbf{x}\cdot\mathbf{r} + \mathbf{r}^2 \right)^{-1/2} = \frac{1}{x} \sum_{n=0}^{\infty} \left(\frac{r}{x} \right)^n P_n\left(\cos(\chi) \right) \tag{13}$$

where χ is the angle between $\mathbf{r}$ and $\mathbf{x}$. Their respective norms are denoted by r and x. In the series expansion (13) the P_n are Legendre polynomials[10]. They are further discussed in appendix D. The series is convergent for all $\mathbf{x}$ such that $r < x$, therefore it does converge if $\mathbf{x}$ is outside a sphere containing the body. This is a classical result of the theory of spherical harmonics [Landau and Lifshitz, 1975, §41].

The potential can now be written as :

$$U(\mathbf{x}, t) = \int_B d^3r\, \frac{G\rho(\mathbf{r}, t)}{x} \sum_{n=0}^{\infty} \left(\frac{r}{x} \right)^n P_n\left(\cos(\chi) \right) \tag{14}$$

$$= \frac{G}{x} \sum_{n=0}^{\infty} \left(\frac{1}{x} \right)^n \int_B d^3r\, \rho(\mathbf{r}, t) r^n\, P_n\left(\cos(\chi) \right) \tag{15}$$

$$= \frac{GM}{x} + \frac{G\,\mathbf{p}\cdot\mathbf{x}}{x^3} + \frac{G}{2}\frac{Q_{ij}x_i x_j}{x^5} + \dots \tag{16}$$

In the above terms of higher order than quadrupole have been neglected. We denote the total mass of the distribution by M.

The dipole moment of the mass distribution is given by (17).

$$\mathbf{p}(t) = \int_B d^3x\, \rho(\mathbf{x}, t)\, \mathbf{x} \tag{17}$$

[10] The Legendre polynomials were introduced in 1782 by Adrien-Marie Legendre for exactly this expansion of the Newtonian potential. [Le Gendre, 1782]

In the planet's proper frame, it vanishes if the mass distribution has a center of symmetry, since all masses are positive and the symmetry entails that the integrand is an uneven function. This is a very good approximation for a planet like Jupiter.

The quadrupole moment of the mass distribution is given by (18), it is a symmetric trace free tensor of rank 2.

$$Q_{ij}(t) = \int_B d^3x\, \rho(\mathbf{x}, t) \left(x_i x_j - \frac{1}{3}\delta_{ij} r^2 \right)$$

To a very good approximation, planets are spherical and they are cylindrically symmetric around their axis of rotation. This shape can be accounted for to reasonably good approximation by the monopole and quadrupole terms in the expansion. The latter accounts for the flattening at the poles as a deviation from spherical shape. Since Q_{ij} is a symmetric real valued tensor it can be brought to principal axes. One of these is the axis of rotation of the planet $\mathbf{z}$, which is also a symmetry axis. The principal value associated with this axis shall be denoted by J_2, then the other two principal values I_1, I_2 associated to axis in the x, y plane are equal, since Q is trace free : $I_1 = I_2 = -1/2\, J_2$.

With these assumptions the potential can be written as :

$$U(\mathbf{x}, t) = \frac{GM}{x} + \frac{G}{2}\frac{Q_{il} x_i x_l}{x^5} + \dots \tag{18}$$

$$\Rightarrow \quad \partial_j U(\mathbf{x}, t) = GM\, \partial_j \frac{1}{x} + \frac{G}{2}\, \partial_j \left(\frac{Q_{il} x_i x_l}{x^5} \right) \tag{19}$$

The gradient $\partial_j U$ of the potential, is used in the formulae for quadrupole light deflection.

Jupiter is the most massive planet in the Solar System and has the largest radius also. A selection of physical data relevant to our experiment is presented in table 4. In the context of light deflection, Jupiter is heavy enough to create observable monopole light deflection. Its quadrupole moment is also large enough for the quadrupole deflection to reach 240 arcsec at its limb (table 1 p. 1588 [Klioner, 2003]). To compute the quadrupole term the direction of Jupiter's rotation axis must be known. In the present work we will assume that it is orthogonal to Jupiter's orbital plane, more sophisticated models have been discussed by the REMAT group Lattanzi and Crosta [2009].

Partly due to its size it is a very bright object ($V \approx -2.7$), this is far below the magnitude threshold of $G = 5.7$ mag, even accounting for the correction of $V \to G$ [Martin Fleitas et al., 2011]. For this reason it cannot directly be observed by Gaia and observations in its vicinity may be impaired [ibidem].

Quantity	Symbol	Unit	Value
radius mean	R_J	$[km]$	$69\,911 \pm 6$
— mean equatorial	R_{Jme}	$[km]$	$71\,492 \pm 4$
mass	M_J	$[10^{24}\,kg]$	1898.13 ± 19
density	ρ_J	$[g\,cm^{-3}]$	1.3262 ± 0.0004
quadrupole moment †	J_2	[1]	$14.7 * 10^{-3}$
period, orbital	T	[yr]	11.862615
— spin	S	[day]	0.41354
magnitude *	V	[mag]	-2.70
grazing ray deflection (monopole)[11]	$\delta\phi$	[arcsec]	0.0163

Table 4: Physical parameters for Jupiter provided by JPL : `http://ssd.jpl.nasa.gov/?planet_phys_par`. († The value for the quadrupole moment J_2 is taken from Fienga et al. [2008] as cited by Zschocke and Klioner [2011]. * The value for V is taken from Martin Fleitas et al. [2011].)

Figure 12: A picture of Jupiter in the visible taken by the Cassini probe. (Credit: NASA/JPL/Space Science Institute; PIA04866)

[11]Calculated using the formula 31, for an observer on Earth or for Gaia's orbit (for the point of closest approach of Jupiter and the observer). Klioner [2003] gives 1620 μarcsecfor monopole deflection by Jupiter

3.3.4 Transformations of the source direction

The source direction is the direction from the observer towards the source, it can be expressed in different reference systems. The source direction undergoes transformations as outlined in Lindegren et al. [1992] and Klioner [2008].

At a given time a star in the Milky Way has a definite position in the BCRS. This direction is defined by the source's astrometric parameters, which to obtain with great accuracy is the point of astrometry. We here study the extent to which light deflection, in particular monopole and quadrupole contributions affect measurement of stellar positions for the Gaia space mission.

The (BCRS) coordinate direction of a sources is the (apparent) Euclidean (3-vector) direction from the barycenter of the Solar System toward the source. It is expressed in the locally Euclidean (or Minkowskian) reference frame of an observer at the barycenter. The notation for it is $\bar{\mathbf{u}}$. It is obtained from the (BCRS) barycentric astrometric parameters of the object by taking into account transformations for secular acceleration, proper motion and parallax.

The natural direction is $\hat{\mathbf{u}}$. It is the direction from a hypothetical observer, who is stationary in BCRS. The transformation from the coordinate direction to the natural direction accounts for the shift of origin from the barycenter of the Solar System to the position of the observer. That is the origin of the natural frame of the satellite (SRS). This vector is obtained by accounting for light deflection ($\Delta\Phi$) by the sun and planets, notably Earth and Jupiter. This term will be considered in the next section 3.3.6. The transformation from $\bar{\mathbf{u}}$ to $\hat{\mathbf{u}}$ is given by:

$$\hat{\mathbf{u}} \quad = \quad \langle\, \bar{\mathbf{u}} + \Delta\Phi \,\rangle = \frac{\bar{\mathbf{u}} + \Delta\Phi}{||\, \bar{\mathbf{u}} + \Delta\Phi \,||} \tag{20}$$

The observable or "proper" direction of a source is denoted $\mathbf{u}$. For Gaia it is the source direction expressed in the CoMRS frame. It is obtained by carrying out the Lorentz transformation accounting for the observer's motion in BCRS. This means that, it is obtained from the natural direction by accounting for stellar aberration due to the barycentric velocity ($\mathbf{v}$) of the satellite.

$$\mathbf{u} \quad = \quad \left\langle\, \hat{\mathbf{u}} + \mathbf{v}\frac{1 + \hat{\mathbf{u}} \cdot \mathbf{v}(c+e)^{-1}}{e} \,\right\rangle \tag{21}$$

where $e = (c^2 - ||\mathbf{v}||^2)^{1/2}$. These equations (20) and (21) are taken from section 5.2 of Lindegren [2001].

3.3.5 Equations of quadrupole light deflection

The differential equations of the null-geodesic light path in the post-Newtonian approximation are (22). The potential and its gradient derived in the previous section are then used to solve them. For a given observed star position, the equations allow to trace the light path back to emission event, that is the location of the source at the moment of emission. For the configurations and bodies we study, the gravitational fields are weak and therefore the "deflection" effect is small. We will calculate the deflection vector of the light path $\Delta\Phi$, its magnitude can be interpreted as the deflection angle. We use the ICRS frame (also called E in Gaia notation), to define vectors. It is a local quasi Cartesian coordinate system [Will, 1993, p. 92].

We discuss the equations given in Crosta and Mignard [2006]. The notation has been adapted to AGISLab notation. Stars will be referred to as "sources". We use the right-handed basis $\mathbf{n}, \mathbf{t}, \mathbf{m}$ which is defined by the light ray arriving from the source as seen in figure 13. The tangent vector to the ray is $\mathbf{t}$, the vector $\mathbf{n}$ points towards the planet along the impact parameter b and $\mathbf{m} = \mathbf{n}\times\mathbf{t}$. The notation for the spin axis of the planet is $\mathbf{z}$. The direction from the observer to the planet is $\mathbf{u}_{\mathrm{p}}$. Crosta and Mignard suppose that the planets are "isolated stationary axisymmetric masses". Hence the formulae we give below are valid in Jupiter's rest frame.

For a light ray passing outside the matter distribution, Crosta and Mignard integrate the following equation:

$$\partial_t^2 x^j_{D\perp} = (1+\gamma)\nabla_\perp U \tag{22}$$

where x^j_D is the relativistic deviation to the zero order (Newtonian) straight line trajectory, and $\nabla_\perp U$ is the projection of the gradient of U (19) onto the plane perpendicular to the light ray. This is the $(\mathbf{n}, \mathbf{m})$ plane shown in figure 13 (b).

The light deflection of the ray is obtained as:

$$\Delta\Phi = \int_{path} \partial_l \mathbf{t}\, dl = \int_{path} (1+\gamma)\nabla_\perp U\, dl \tag{23}$$

with the following expression for the gradient:

$$\begin{aligned} \nabla_\perp U \;=\; & \left[-\frac{b}{r}\left(-\frac{M}{r^2} + \frac{3M}{r^4}\, J_2 R^2\, \frac{5\cos^2(\chi)-1}{2} \right) - \frac{3M}{r^4}\, J_2 R^2\, \cos(\chi)\, (\mathbf{z}\cdot\mathbf{n}) \right] \mathbf{n} \\ & - \frac{3M}{r^4}\, J_2 R^2\, \cos(\chi)\, (\mathbf{z}\cdot\mathbf{m})\, \mathbf{m} \end{aligned} \tag{24}$$

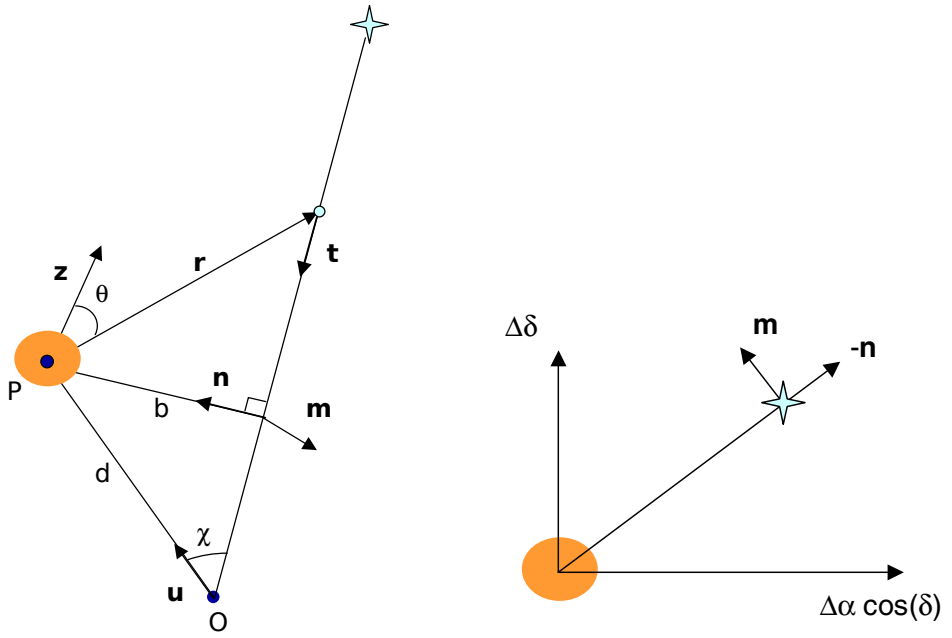

(a) The geometry of light deflection due to a planet (P): the spin axis of the planet **z** is out of the plane; **t** represents the unit tangent vector from a distant star (S) to the observer (O) on the unperturbed light trajectory; **u** is the unit direction from O to P along their distance d ; finally, χ is the angle $\widehat{SOP}$, and b is the impact parameter.

(b) Light deflection by a planet: tangent plane on the sky. The position of the star is displaced both in the radial ($-\mathbf{n}$) and orthoradial **m** directions. The spin axis of the planet **z** (not shown here) does not lie in this plane in general.

Figure 13: Figures describing the light deflection geometry from Crosta and Mignard [2006]

Upon integration of equation (23) along the *path* from the source to the observer the projection of the deflection vector onto the $(\mathbf{n}, \mathbf{m})$ plane is obtained. For its components Crosta and Mignard [2006] obtain:

$$\Delta\Phi = \Delta\Phi_1\,\mathbf{n} + \Delta\Phi_2\,\mathbf{m} \tag{25}$$

$$\begin{aligned}\Delta\Phi_1 = {} & (1+\gamma)\,\frac{GM}{c^2}\,\frac{1}{ab}\left((1+\cos\chi) + J_2\,\frac{R^2}{a^2b^2}\left[\;(1+\cos\chi+\frac{1}{2}\cos\chi\sin^2\chi)\right.\right.\\ & -2\,(1+\cos\chi+\frac{1}{2}\cos\chi\sin^2\chi+\frac{3}{4}\cos\chi\sin^4\chi)(\mathbf{n}\cdot\mathbf{z})^2\\ & +(\sin^3\chi-3\sin^5\chi)(\mathbf{n}\cdot\mathbf{z})(\mathbf{t}\cdot\mathbf{z})\\ & \left.\left.-(1+\cos\chi+\frac{1}{2}\cos\chi\sin^2\chi-\frac{3}{2}\cos\chi\sin^4\chi)(\mathbf{t}\cdot\mathbf{z})^2\;\right]\right)\end{aligned} \tag{26}$$

$$\begin{aligned}\Delta\Phi_2 = {} & (1+\gamma)\,\frac{GM}{c^2}\,J_2\,\frac{R^2}{a^3b^3}\left(\;2(1+\cos\chi+\frac{1}{2}\cos\chi\sin^2\chi)\;(\mathbf{n}\cdot\mathbf{z})\;(\mathbf{m}\cdot\mathbf{z})\right.\\ & \left.+\sin^3\chi\;(\mathbf{m}\cdot\mathbf{z})\;(\mathbf{t}\cdot\mathbf{z})\;\right)\end{aligned} \tag{27}$$

The parameters in this formula are :

- R is the equatorial radius of the deflecting object, M its mass and J_2 the quadrupole moment.
- where d as shown in figure 13 (a) is the distance from Gaia to the deflecting object, measured in astronomical units (AU)

- b is the impact parameter, the distance from the planet to the trajectory of the light ray, it is also measured in AU. We have: $b = d\sin(\chi)$
- χ if the angle between the directions from the observer toward the source and the planet, we have $\chi = (\widehat{\mathbf{u}_\mathrm{p}, -\mathbf{t}})$ and $\cos(\chi) = -(\mathbf{u}_\mathrm{p} \cdot \mathbf{t})$.
- a is the value of 1 AU in meters as given in table 10 in appendix C.

An interesting particular case of formula (25) is the limit $J_2 \to 0$.

$$\Delta\Phi_1 \;\to\; (1+\gamma)\,\frac{GM}{c^2}\,\frac{1}{ab}\,(1+\cos\chi) \tag{28}$$

$$\Delta\Phi_2 \;\to\; 0 \tag{29}$$

$$\Rightarrow \Delta\Phi \;\to\; (1+\gamma)\,\frac{GM}{c^2}\,\frac{1}{ab}\,(1+\cos\chi)\,\mathbf{n} \;=\; (1+\gamma)\,\frac{GM}{c^2}\,\frac{1}{ad}\left(\frac{1+\cos\chi}{\sin\chi}\right)\mathbf{n} \tag{30}$$

We obtain the expected equation for the monopole light deflection:

$$||\Delta\Phi|| \to \delta_m\phi = (1+\gamma)\,\frac{GM}{c^2 ad}\left(\frac{1+\cos\chi}{\sin\chi}\right) = (1+\gamma)\,\frac{GM}{c^2 ad}\,\mathrm{cotan}\left(\frac{\chi}{2}\right) \tag{31}$$

The monopole deflection angle $\delta_m\phi$ (with $\gamma = 1$) was used by Eddington for the solar light deflection experiment to confirm general relativity. Its value is 1.75 arcsec for grazing rays. The formula was also used in Hipparcos data reduction for light deflection by the Sun and Earth [Lindegren et al., 1992].

In the following we call quadrupole term the quantity: $\Delta_q\Phi = (\Delta\Phi_1 - \delta_m\phi)\,\mathbf{n} + \Delta\Phi_2\,\mathbf{m}$.

3.3.6 The quadrupole efficiency factor and derivatives

A further equation is needed for numerical resolution of the quadrupole light deflection equations in the AGIS framework. Therefore we introduce the quadrupole efficiency factor and deduce equations (37) and (38). We then obtain the equation (50) for the derivatives of the source direction vector, as required by the AGIS scheme. This refers to the method outlined in section 4.1 of report 2.

The formulae (26) and (27) being heavy, we introduce the following notation:

$$\mathcal{A} \;=\; (1+\gamma)\,\frac{GM}{c^2}\,\frac{1}{ab} \tag{32}$$

$$\mathcal{B} \;=\; J_2\,\frac{R^2}{a^2b^2} \tag{33}$$

$$\mathcal{C} \;=\; \frac{GM}{c^2}\,\frac{1}{a^2d^2}\,\frac{1}{1-\cos(\chi)} \tag{34}$$

$$\begin{aligned} f_1(\chi) \;=\;& (1+\cos\chi+\frac{1}{2}\cos\chi\sin^2\chi) \\ & -2\,(1+\cos\chi+\frac{1}{2}\cos\chi\sin^2\chi+\frac{3}{4}\cos\chi\sin^4\chi)(\mathbf{n}\cdot\mathbf{z})^2 \\ & +(\sin^3\chi-3\sin^5\chi)(\mathbf{n}\cdot\mathbf{z})(\mathbf{t}\cdot\mathbf{z}) \\ & -(1+\cos\chi+\frac{1}{2}\cos\chi\sin^2\chi-\frac{3}{2}\cos\chi\sin^4\chi)(\mathbf{t}\cdot\mathbf{z})^2 \end{aligned} \tag{35}$$

$$\begin{aligned} f_2(\chi) \;=\;& 2(1+\cos\chi+\frac{1}{2}\cos\chi\sin^2\chi)\;(\mathbf{n}\cdot\mathbf{z})\;(\mathbf{m}\cdot\mathbf{z}) \\ & +\sin^3\chi\;(\mathbf{m}\cdot\mathbf{z})\;(\mathbf{t}\cdot\mathbf{z}) \end{aligned} \tag{36}$$

The quadrupole efficiency factor (QEF) is denoted by ε, as in [Crosta and Mignard, 2006]. It scales the quadrupole term in equations (26) and (27). These equations become:

$$\Delta\Phi_1 = \mathcal{A}\ [\ (1+\cos\chi)\ +\ \varepsilon\,\mathcal{B}\ f_1(\chi)\ ] \tag{37}$$
$$\Delta\Phi_2 = \varepsilon\,\mathcal{A}\,\mathcal{B}\ f_2(\chi) \tag{38}$$

Equation (25) still holds, the total deflection is $\Delta\Phi = \Delta\Phi_1\,\mathbf{n} + \Delta\Phi_2\,\mathbf{m}$.

The derivatives required by the AGIS framework are those of the natural source direction $\hat{\mathbf{u}}$ with respect to ε. Here we give the detail of their calculation.

$$\frac{\partial\,\hat{\mathbf{u}}}{\partial\varepsilon} = \partial_\varepsilon\,\hat{\mathbf{u}} \tag{39}$$
$$= \frac{\partial_\varepsilon\Delta\Phi}{||\ \bar{\mathbf{u}}+\Delta\Phi\ ||}\ +\ (\bar{\mathbf{u}}+\Delta\Phi)\ \partial_\varepsilon\left(\frac{1}{||\ \bar{\mathbf{u}}+\Delta\Phi\ ||}\right) \tag{40}$$
$$= \frac{(\ \partial_\varepsilon\Delta\Phi_1\ )\ \mathbf{n} + (\ \partial_\varepsilon\Delta\Phi_2\ )\ \mathbf{m}}{||\ \bar{\mathbf{u}}+\Delta\Phi\ ||}\ +\ (\bar{\mathbf{u}}+\Delta\Phi)\ \partial_\varepsilon\left(\frac{1}{||\ \bar{\mathbf{u}}+\Delta\Phi\ ||}\right) \tag{41}$$

Where we use the notation: $\partial_x = \frac{\partial}{\partial x}$. It follows:

$$\partial_\varepsilon\Delta\Phi = (\ \partial_\varepsilon\Delta\Phi_1\ )\ \mathbf{n} + (\ \partial_\varepsilon\Delta\Phi_2\ )\ \mathbf{m} = \mathcal{A}\,\mathcal{B}\ f_1(\chi)\mathbf{n}\ +\ \mathcal{A}\,\mathcal{B}\ f_2(\chi)\mathbf{m} \tag{42}$$

$$\partial_\varepsilon\left(\frac{1}{||\ \bar{\mathbf{u}}+\Delta\Phi\ ||}\right) = -\left(\frac{1}{||\ \bar{\mathbf{u}}+\Delta\Phi\ ||^2}\right)\ \partial_\varepsilon\,||\ \bar{\mathbf{u}}+\Delta\Phi\ || \tag{43}$$

$$||\ \bar{\mathbf{u}}+\Delta\Phi\ || = \sqrt{\bar{\mathbf{u}}^2+\Delta\Phi^2\ +\ 2\ \bar{\mathbf{u}}\cdot\Delta\Phi} \tag{44}$$
$$\partial_\varepsilon||\ \bar{\mathbf{u}}+\Delta\Phi\ || = \frac{1}{2}\ \frac{1}{||\ \bar{\mathbf{u}}+\Delta\Phi\ ||}\left(\partial_\varepsilon\left(\Delta\Phi^2\right)+\partial_\varepsilon\,2\,\bar{\mathbf{u}}\cdot\Delta\Phi\right) \tag{45}$$
$$\partial_\varepsilon||\ \bar{\mathbf{u}}+\Delta\Phi\ || = \frac{1}{2}\ \frac{1}{||\ \bar{\mathbf{u}}+\Delta\Phi\ ||}\left(\,2\,\Delta\Phi\cdot\partial_\varepsilon\Delta\Phi+\ 2\,\bar{\mathbf{u}}\cdot\ \partial_\varepsilon\,\Delta\Phi\,\right) \tag{46}$$
$$= \frac{(\bar{\mathbf{u}}+\Delta\Phi)\cdot\partial_\varepsilon\,(\,\Delta\Phi\,)}{||\ \bar{\mathbf{u}}+\Delta\Phi\ ||} \tag{47}$$

Thus:

$$\partial_\varepsilon\,\hat{\mathbf{u}} = \frac{\partial_\varepsilon\Delta\Phi}{||\ \bar{\mathbf{u}}+\Delta\Phi\ ||} + (\bar{\mathbf{u}}+\Delta\Phi)\ \partial_\varepsilon\left(\frac{1}{||\ \bar{\mathbf{u}}+\Delta\Phi\ ||}\right) \tag{48}$$
$$= \frac{\partial_\varepsilon\Delta\Phi}{||\ \bar{\mathbf{u}}+\Delta\Phi\ ||}\ +\ (\bar{\mathbf{u}}+\Delta\Phi)\left(\ -\left(\frac{1}{||\ \bar{\mathbf{u}}+\Delta\Phi\ ||^2}\right)\ \frac{(\bar{\mathbf{u}}+\Delta\Phi)\cdot\partial_\varepsilon\,(\,\Delta\Phi\,)}{||\ \bar{\mathbf{u}}+\Delta\Phi\ ||}\right) \tag{49}$$

$$\partial_\varepsilon\,\hat{\mathbf{u}} = \frac{\partial_\varepsilon\Delta\Phi}{||\ \bar{\mathbf{u}}+\Delta\Phi\ ||}\ -\ (\bar{\mathbf{u}}+\Delta\Phi)\ \frac{(\bar{\mathbf{u}}+\Delta\Phi)\cdot\partial_\varepsilon\Delta\Phi}{||\ \bar{\mathbf{u}}+\Delta\Phi\ ||^3} \tag{50}$$

This final expression (50), is the analytic formula for the derivative in the case of a single deflecting body. In the case of multiple deflecting bodies their contributions have to be added as: $\hat{\mathbf{u}}' = \bar{\mathbf{u}} + \Sigma_i\Delta\Phi_i$ and every body may have its own QEF ε_i. In the case of solar system objects and the configuration of Gaia which does not observe close to the Sun, it is sufficiently accurate to calculate derivatives in the approximation of a single body, treat each contribution separately since $||\ \bar{\mathbf{u}}+\Sigma_i\Delta\Phi_i\ || \approx ||\ \bar{\mathbf{u}}\ ||$. This discussion is relegated to section 3.4.

The analog of (50) for the monopole term and gamma is (51). In which we use the heliocentric position of Gaia $\mathbf{r}$, the notation $\mathbf{u_1} = \bar{\mathbf{u}} + \Delta\Phi$ and $u_1 = ||\ \mathbf{u_1}\ ||$.

Next we compare this expression to a further approximation (52), which was used for the derivatives in PPN γ for Hipparcos [Lindegren et al., 1992] and in AGISLab [Hobbs et al., 2010].

$$\frac{\partial\,\hat{\mathbf{u}}}{\partial\gamma} = -\mathcal{C}\,\frac{1}{u_1^3}\,\big(\,(1+\gamma)\,\mathcal{C}\,\mathbf{r}^2+(\mathbf{r}\cdot\mathbf{u})\,\big)\,\mathbf{u_1}+\frac{1}{u_1}\,\mathcal{C}\,\mathbf{r} \tag{51}$$

$$\frac{\partial\,\hat{\mathbf{u}}}{\partial\gamma} \approx (\mathbf{r}\;-\;\bar{\mathbf{u}}(\bar{\mathbf{u}}\cdot\mathbf{r}))\,\frac{GMc^{-2}}{r(r+\bar{\mathbf{u}}\cdot\mathbf{r})} \tag{52}$$

In analogy to (52) we would like to write for $\partial_\varepsilon\,\hat{\mathbf{u}}$:

$$\partial_\varepsilon\,\hat{\mathbf{u}} = \partial_\varepsilon\Delta\Phi\;-\;(\bar{\mathbf{u}}+\Delta\Phi)\,\partial_\varepsilon(\bar{\mathbf{u}}\cdot\Delta\Phi) \tag{53}$$

The derivation of equation (52) uses Taylor expansions. Knowing that the deflection term $\Delta\Phi$ is small (in most observable cases), we can rewrite (20):

$$\begin{aligned}
\hat{\mathbf{u}} &= \frac{\bar{\mathbf{u}}+\Delta\Phi}{||\,\bar{\mathbf{u}}+\Delta\Phi\,||} && (54)\\
&= (\,\bar{\mathbf{u}}+\Delta\Phi\,)\,\big(\,\bar{\mathbf{u}}^2+2\,\bar{\mathbf{u}}\cdot\Delta\Phi+\Delta\Phi^2\,\big)^{-\frac{1}{2}}\\
&= (\,\bar{\mathbf{u}}+\Delta\Phi\,)\,(\,1+2\,\bar{\mathbf{u}}\cdot\Delta\Phi+o(||\Delta\Phi||)\,)^{-\frac{1}{2}}\\
&\approx (\,\bar{\mathbf{u}}+\Delta\Phi\,)\left(\,1-\frac{1}{2}\,2\,\bar{\mathbf{u}}\cdot\Delta\Phi+o(||\Delta\Phi||)\,\right)\\
&\approx \bar{\mathbf{u}}+\Delta\Phi-\bar{\mathbf{u}}\,(\bar{\mathbf{u}}\cdot\Delta\Phi)-\Delta\Phi(\,\bar{\mathbf{u}}\cdot\Delta\Phi)+o(||\Delta\Phi||)\\
&\approx \bar{\mathbf{u}}+\Delta\Phi-\bar{\mathbf{u}}\,(\bar{\mathbf{u}}\cdot\Delta\Phi)+o(||\Delta\Phi||)\\
&\approx \bar{\mathbf{u}}+(1-\bar{\mathbf{u}}\,\bar{\mathbf{u}}^T)\Delta\Phi+o(||\Delta\Phi||) && (55)
\end{aligned}$$

where $\bar{\mathbf{u}}^2=1$ and $\Delta\Phi(\,\bar{\mathbf{u}}\cdot\Delta\Phi)=o(||\Delta\Phi||)$

Upon deriving (55) with respect to ε:

$$\begin{aligned}
\partial_\varepsilon\,\hat{\mathbf{u}} &\approx \partial_\varepsilon\bar{\mathbf{u}}+\partial_\varepsilon\,\big(\,(1-\bar{\mathbf{u}}\,\bar{\mathbf{u}}^T)\Delta\Phi\,\big) && (56)\\
&\approx 0+(1-\bar{\mathbf{u}}\,\bar{\mathbf{u}}^T)\,\partial_\varepsilon\Delta\Phi\\
\partial_\varepsilon\,\hat{\mathbf{u}} &\approx (1-\bar{\mathbf{u}}\,\bar{\mathbf{u}}^T)\,\partial_\varepsilon\Delta\Phi && (57)\\
\partial_\varepsilon\,\hat{\mathbf{u}} &\approx \partial_\varepsilon\Delta\Phi-\bar{\mathbf{u}}\;(\,\bar{\mathbf{u}}\cdot\partial_\varepsilon\Delta\Phi\,) && (58)
\end{aligned}$$

Alternatively, deriving (55) with respect to γ:

$$\begin{aligned}
\partial_\gamma\,\hat{\mathbf{u}} &\approx \partial_\gamma\bar{\mathbf{u}}+\partial_\gamma\,\big(\,(1-\bar{\mathbf{u}}\,\bar{\mathbf{u}}^T)\Delta\Phi\,\big) && (59)\\
&\approx 0+(1-\bar{\mathbf{u}}\,\bar{\mathbf{u}}^T)\,\partial_\gamma\Delta\Phi\\
\partial_\gamma\,\hat{\mathbf{u}} &\approx (1-\bar{\mathbf{u}}\,\bar{\mathbf{u}}^T)\,\partial_\gamma\Delta\Phi && (60)\\
\partial_\gamma\,\hat{\mathbf{u}} &\approx \partial_\gamma\Delta\Phi-\bar{\mathbf{u}}\;(\,\bar{\mathbf{u}}\cdot\partial_\gamma\Delta\Phi\,) && (61)
\end{aligned}$$

These different expressions for the derivatives have been implemented and tested in AGISLab. The results of the different formulae are compared in the next section.

3.4 Testing the derivatives for QEF ε

3.4.1 Design choices

In this section we discuss the testing strategy used in AGISLab. We first have started to implement the equations discussed above in AGISLab. Then we have developed a set of simple stand-alone tests.

The objective is to test the formulae for quadrupole deflection. For the purpose of testing the formulae for light deflection up to quadrupole order and the source direction derivatives, we have adopted a design using three classes: QuadrupoleDerivatives, QuadrupoleDerivativesTest and QuadrupoleDerivativesStructuredData. Their relations are shown in figure 7.

The class QuadrupoleDerivatives implements the formulae to be tested. The monopole deflection formula (31) and the equation (37) and (38) which includes the quadrupole terms are implemented. For the derivatives we have implemented three versions for both $\partial_\varepsilon \hat{\mathbf{u}}$ and $\partial_\gamma \hat{\mathbf{u}}$. For $\partial_\varepsilon \hat{\mathbf{u}}$ we calculate (50), (58) and a numerical derivative described below (62). For $\partial_\gamma \hat{\mathbf{u}}$ we calculate (52), (61) and a numerical derivative defined by (63).

QuadrupoleDerivativesTest implements a set of tests described below. The auxiliary class QuadrupoleDerivativesStructuredData is a data structure designed to store parameters for calculations, such as Gaia's and Jupiter's positions and the $\mathcal{A}, \mathcal{B}$, f_1, f_2 factors in (37) and (38) which may be reused for the evaluation of the derivatives.

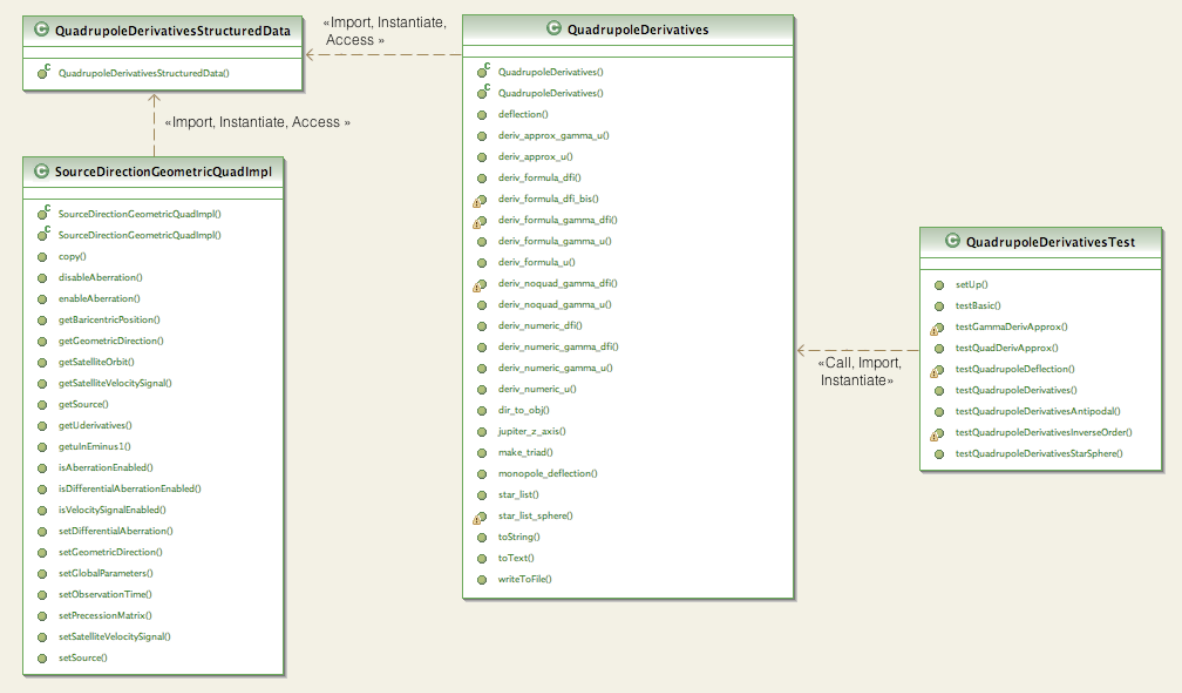

Figure 14: The UML diagram of the relations between the classes QuadrupoleDerivatives, QuadrupoleDerivativesTest and QuadrupoleDerivativesStructuredData.

In the next step, we turned toward the implementation of the calculations in AGISLab. The light deflection calculation in AGISLab is handled by the SourceDirection interface. There is a pre-existing implementation of SourceDirection called SourceDirectionGeometricImpl, implemented by Hobbs et al. [2010]. This calculates the "proper source direction" starting from observation data and it uses a model for monopole light deflection for the Sun and planets. This is very similar to the model that was used in Hipparcos data processing [Lindegren et al., 1992]. We will subsequently call this implementation the "old" model.

The implementation we are devising is SourceDirectionGeometricQuadImpl which will take into account the light deflection terms up to quadrupole order. It implements the validated

equations (37) and (38) and the derivatives (50) for QEF ε and (51) for PPN γ. An intermediary implementation SourceDirectionGeometricMonoImpl has been implemented for the purpose of comparing results to those of the "old" model. It is an early version of SourceDirectionGeometricQuadImpl. It uses the new formalism and derivative equations for PPN γ, We have paid attention to writing documentation for the implemented methods. The final design of this class will be discussed later. We call this the "new" model. Its first test is to reproduce the monopole results (convergence plots) for the Sun and Jupiter.

3.4.2 Testing strategy

The main type of test we have implemented is designed to compare the results of different derivative and deflection calculations. To obtain these values in different configurations the following steps have to be carried out.

Before any test method runs the main parameters are set (see table 6 for values). The physical constants provided by the Gaia Parameter Database were used.

Then the positions of Jupiter and Gaia are calculated from ephemeris and the star list is generated. For these tests the position of Jupiter was chosen arbitrarily, a set of different coordinates has been tested and it was shown that they have no effect on the results. This is to be expected as the effect is not coordinate dependent, it depends only on the relative position of the star, Jupiter and Gaia. Later Jupiter's position is obtained from the ephemeris (SolarSystemEphemeris) implemented in GaiaTools.

We generate stars near Jupiter (for instance the one shown in figure 15), by creating a rectangular field of stars, near some object (e.g. Jupiter) using two parameters: the smallest angle between two stars (in radian), and the number of stars on one side of the rectangle. Finally the deflection and/or derivatives are calculated, compared to numerical derivatives and written to an output file.

We chose to implement monopole and quadrupole calculations in separate methods as this is required later for use with AGISLab. For the numerical derivative $\Delta_\varepsilon \hat{\mathbf{u}}_*$ for a star we use the symmetrised numerical derivative, defined as:

$$\Delta_\varepsilon \hat{\mathbf{u}}_*(\varepsilon) = \frac{\hat{\mathbf{u}}_*(\varepsilon + \Delta\varepsilon/2) - \hat{\mathbf{u}}_*(\varepsilon - \Delta\varepsilon/2)}{\Delta\varepsilon} = \frac{\Delta\Phi_*(\varepsilon + \Delta\varepsilon/2) - \Delta\Phi_*(\varepsilon - \Delta\varepsilon/2)}{\Delta\varepsilon} \tag{62}$$

This numerical scheme has been implemented for both derivatives in QEF ε and PPN γ, to allow verification.

$$\Delta_\gamma \hat{\mathbf{u}}_*(\gamma) = \frac{\hat{\mathbf{u}}_*(\gamma + \Delta\gamma/2) - \hat{\mathbf{u}}_*(\gamma - \Delta\gamma/2)}{\Delta\gamma} = \frac{\Delta\Phi_*(\gamma + \Delta\gamma/2) - \Delta\Phi_*(\gamma - \Delta\gamma/2)}{\Delta\gamma} \tag{63}$$

Different test cases were implemented to verify distinct aspects of the implementation of the formulae. They are shown in table 5.

Test 1	compare	the analytical and numerical derivative formulae
Test 2	unit test	check the formal validity of the algorithm
Test 3	compare	the deflection norms (monopole, quadrupole, total)
Test 4	compare	the analytical and numerical deflection formulae at the antipode of Jupiter
Test 5	compare	the quadrupole (ε) derivatives : analytical, approximate and numerical
Test 6	compare	monopole (γ) derivatives : analytical, approximate and numerical

Table 5: The different test cases for the derivative equations and deflection formulae.

We will discuss the most pertinent results from these tests in the paragraphs that follow.

3.4.3 Results from the stand-alone test set

The tests allowed us to get a feeling for the magnitude and variability of the quadrupole deflection term. In the tests of the deflection equations (37) and (38) we have computed the quadrupole and monopole deflection terms and compared them to the established results. Our numerical values agreed with the ones found in the literature [Crosta and Mignard, 2006, Klioner, 2003]. The monopole term for Jupiter is of the order of 16.3 milli arcsec for a grazing ray (see table 7). The quadrupole term for a grazing ray is about 200 μarcsec in agreement with [Klioner, 2003]. The unit tests allowed us to trace the calls made by the algorithms and validate the steps in the calculation scheme. The tests of the different derivative formulae (tests 4 , 5 , 6 in table 5) agreed well, for the chosen values of the parameter $\delta = \Delta\varepsilon$ or $\delta = \Delta\gamma$. In general for stars outside Jupiter's radius a value of $\delta = 0.001$ for the numerical step size is sufficient for 6 decimals of agreement with the analytical and numerical derivative formulae. The agreement of the analytical with approximate formulae is of the same order. This warrants the approximations mentioned in 3.3.6.

Far away from Jupiter, the quadrupole deflection term (25) is expected to be negligible since it is proportional to the inverse of the cube of the impact parameter b : $\Delta\Phi \propto (1/b^3)$ according to (27) . The derivative of the source direction (50) would then be small as well, because $|| \bar{\mathbf{u}} + \Delta\Phi || \approx ||\bar{\mathbf{u}}|| \approx 1$ and $\partial_\varepsilon \Delta\Phi \propto \mathcal{AB} \propto (1/b^3)$ in virtue of (42) . This has been tested at the antipode of Jupiter, i.e. at the point on the celestial sphere diametrically opposite to Jupiter (test case 3). At the antipode of Jupiter the deflection and derivatives are zero exactly due to symmetry reasons. In the immediate surroundings of the antipode (20 arcsec), the norm of the total deflection is of the order of 10^{-16} rad (or 10^{-5} μarcsec) and the norm of the derivative in ε is 10^{-26} rad (or 10^{-15} μarcsec). These are very small compared to the values in the vicinity of Jupiter, at 20 arcsec the norm of the total deflection is of the order of 10^{-7} rad (or 10^{-2} arcsec) and the norm of the derivative in ε is 10^{-9} rad (or 10^{-4} arcsec). For a grazing ray (observed from earth) we obtain : about 17 milliarcsec for the total deflection in agreement with [Klioner, 2003]. These values are the results of tests 3, 4, 5 in table 5.

Quantity	Unit	Value
Jupiter's apparent radius	[arcsec]	≈ 20
angle between stars	[arcsec]	20
total number of stars	[ND]	$n^2 = 16$
numerical step size (δ)	[ND]	0.001
grazing ray deflection (monopole)	[arcsec]	0.0163
maximal level of the quadrupole term[12]	[μarcsec]	240
maximal level of $\partial_\varepsilon \hat{\mathbf{u}}$	[arcsec]	10^{-4}
minimal level of $\partial_\varepsilon \hat{\mathbf{u}}$	[arcsec]	$< 10^{-15}$
maximal level of the derivative in γ	[arcsec]	10^{-3}
minimal level of the derivative in γ	[arcsec]	$< 10^{-11}$

Table 6: Test parameters for the first tests of the implementation of quadrupole light deflection terms and derivates. (We write [ND] to indicate that the quantity in question has no dimension.)

For the derivative in PPN γ for Jupiter test 5 (table 5), the behaviour is similar. The results are shown in table 6.

[12] This is the value given in table 1 p. 1588 [Klioner, 2003].

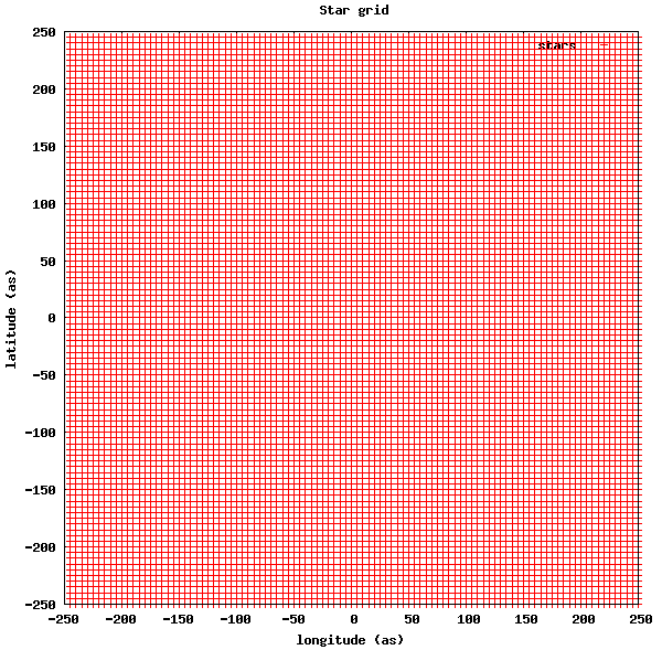

Figure 15: Grid of stars (100×100) used for the derivative test, the center of the grid is the position of the deflecting object (Jupiter) in the spherical coordinate system, projected onto the plane tangent to the celestial sphere in the direction of the deflecting object. [image generated with Gnuplot]

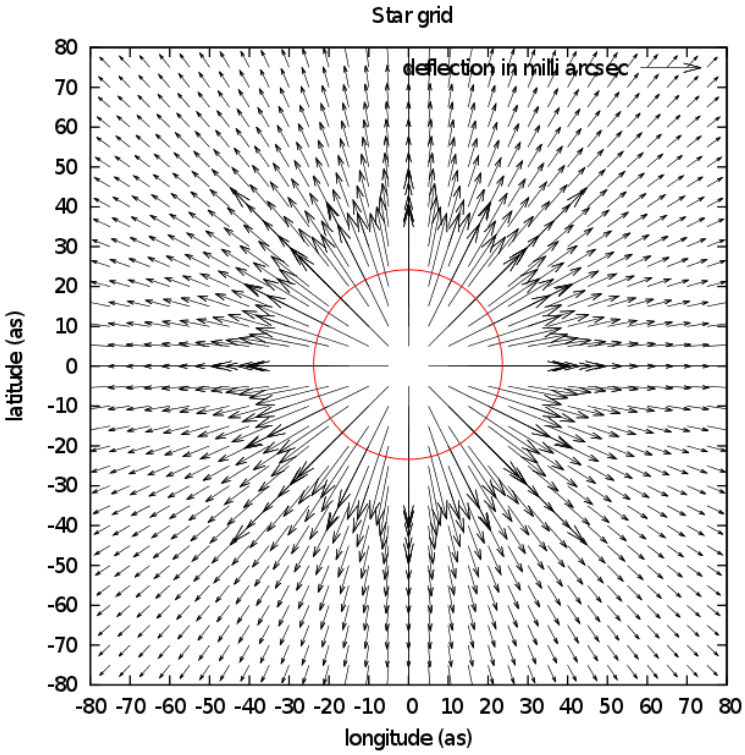

Figure 16: Monopole deflection for the same stars (100×100) as in figure 15. This shows a zoom on the inner 160 arcsec. Jupiter is located at the center of the field and is represented by a red circle of radius 24 arcsec. (The scale of the arrows is in milli arcsec, i.e. they have been scaled up by a factor of one thousand compared to the angular scale.) [image generated with Gnuplot]

3.4.4 Testing the convergence of the new setup in AGISLab

After these preliminary tests, we have implemented the derivatives in the SourceDirectionQuadImpl. We tested the convergence of the new scheme to calculate light deflection, we restricted the calculation to the monopole term using the new formalism (25) up to monopole order (31) and the derivative equation (51) for PPN γ. The results of our new runs agree with runs using the old formalism to a good precision, as shown in table 7.

Figure 17 shows the convergence plot for the global parameters, PPN γ of the Sun and PPN γ of Jupiter, in the old configuration. Figure 18 shows the convergence plot for the global parameters, PPN γ of the Sun and PPN γ of Jupiter, in the new set up.

Both runs use the same setup parameters, specified in a properties file. The essential ones are scale parameter: $S = 0.020$ and the reference number of sources: nSources $= 10^6$, which results in 20 000 sources. We do 50 iterations using a conjugate gradient scheme with 5 years of data starting in 2014.

Moreover we tried to make the simulation as realistic as possible despite the small scale parameter. In these simulations we use bright stars, we chose to use stars of magnitude $G = 13$ only. The model includes Observation noise as described in de Bruijne [2009]. It accounts for the estimated AL and AC location-estimation performance of Gaia. This is a function of magnitude and affects the weight (w) of each observed star in equation (1).

The initial error in PPN γ is set to a 0.1 deviation. The value initially assumed by AGISLab is therefore $\gamma = 1.1$ for both Jupiter and the Sun. These runs also include initial errors in attitude and source parameters, defined by the run properties.

Quantity	Value
scale parameter (S)	0.020
number of stars	20 000
number of iterations	50
start date	J2014
initial error in PPN γ	+0.1
$\mathrm{Err}_{\mathrm{Sun}}(\gamma_{\mathrm{S}})$ (old)	$-5.516 * 10^{-5}$
$\mathrm{Err}_{\mathrm{Sun}}(\gamma_{\mathrm{S}})$ (new)	$-5.501 * 10^{-5}$
$\mathrm{Err}_{\mathrm{Jup}}(\gamma_{\mathrm{J}})$ (old)	$-2.322 * 10^{-4}$
$\mathrm{Err}_{\mathrm{Jup}}(\gamma_{\mathrm{J}})$ (new)	$-2.374 * 10^{-4}$

Table 7: Test parameters and results for the two runs of monopole light deflection terms and derivates for figures 17 and 18.

The results shown in table 7 and the numbers given at the bottom of the figures below are the values of the errors in "global parameters" PPN γ for the Sun, PPN γ for Jupiter, and QEF ε for Jupiter, and their "updates" at the end of the last iteration, iteration 50 in this case. The errors are defined by the following relations:

$$\mathrm{Err}_{\mathrm{Sun}}(\gamma) = \gamma_{\mathrm{S}} - 1 \tag{64}$$

$$\mathrm{Err}_{\mathrm{Jup}}(\gamma) = \gamma_{\mathrm{J}} - 1 \tag{65}$$

We are calculating two estimates for PPN γ, to asses the precision with which it can be determined using a given method.

The plots in figures 17 and 18 show an oscillating behaviour initially, as the conjugate gradient algorithm tries to find the optimum solution. As the errors oscillate around zero and assume both positive and negative values, it is not possible to generate logarithmic plots with negative values of the errors $\mathrm{Err}_{\mathrm{Sun}}$ and $\mathrm{Err}_{\mathrm{Jup}}$. This issue will be addressed in future revisions of AGISLab.

The larger amplitude of the oscillations for Jupiter is due to the fact that the monopole deflection is weaker than the Sun's. Since Jupiter is about a thousand times less massive, but only about one tenth smaller in radius than the Sun, the grazing ray deflection is smaller by a factor of one hundred as given in table 8. For an observer in the vicinity of the Earth and even for Gaia, these are the maximal values of light deflection observable for the solar system objects. A discussion of this is given in (table 1 p. 1588) [Klioner, 2003]. The monopole deflection decreases with the separation between the source, since it is proportional to the inverse of the impact parameter $b = d \sin\chi$. For the deflection of the Sun as observed by Gaia in the opposite direction is still larger than the expected Gaia precision[13]. For Jupiter the effect is weaker. At optimal precision of the measurements half the sky could contribute to the determination of PPN γ using Jupiter's monopole deflection.

Thus many more observations constrain the value of PPN γ for the Sun than for Jupiter, which explains the smaller oscillations. Each star contributes for the Sun, but for Jupiter only those stars in the vicinity of Jupiter when it is observed by Gaia contribute. This is also responsible for the difference in the converged values of the errors.

Quantity	Unit	Jupiter	Sun
Equatorial radius	[m]	$7.149 \cdot 10^7$	$6.960 \cdot 10^8$
Angular radius	[arcsec]	19	960
Distance to the observer	[AU]	4.2	1
Mass	[kg]	$1.898 \cdot 10^{27}$	$1.988 \cdot 10^{30}$
Monopole grazing ray light deflection	[arcsec]	0.0163	1.75

Table 8: Comparison of the monopole deflection at the equator by the Sun and Jupiter. With PPN $\gamma = 1$ and the observer in the vicinity of Earth. Deflection calculated using (31) and rounded parameters from the Gaia Parameter Database (`http://gaia.esac.esa.int/gpdb`).

The agreement is to 2.3 % of the error value for Jupiter's PPN γ obtained with the original AGIS implementation. The absolute difference is $|\Delta\mathrm{Err}_{\mathrm{Jup}}| = 5.3 * 10^{-6}$.

For the Sun, the agreement is to 0.27 % of the Sun's PPN γ error value obtained with the original AGIS implementation. The absolute difference is $|\Delta\mathrm{Err}_{\mathrm{Sun}}| = 1.5 * 10^{-7}$.

There is also a difference in the updates for the errors of Jupiter (of the order of 10^{-6}) and the Sun (of the order of 10^{-7}). This is of the order of the numerical precision of the calculation. For both the Sun and Jupiter, we can conclude that the error has converged at the level of 10^{-5} and 10^{-4} respectively. However since the updates are of the order of the disagreement between the two methods, we cannot say how large it really is, but it must be smaller than the value given. With larger runs better precision can be reached.

This test shows that the new implementation gives correct results up to numerical precision and the limitation imposed by a small scale parameter. The results are good for such small simulations. We plan to run bigger simulations and implement the quadrupole calculation, to study the sensitivity to which Gaia can probe this effect.

[13] At the antipode exactly, at 180° from the center of the Sun, the effect is precisely zero for symmetry reasons. However even close to the antipode the Sun's monopole effect must still be considered for high precision astrometry. At 179° for instance, we obtain $\delta_m\phi = 35.5$ μarcsec (for $\gamma = 1$) according to (31) and the constants given above. This is in agreement with table 1 p. 1588 [Klioner, 2003]which indicates that the effect is larger than 10 μarcsec for an angular separation of 180° between the source and the deflecting body. For Jupiter the effect falls below the 1μarcsec limit at 90°, this can also be found in table 1 in [Klioner, 2003].

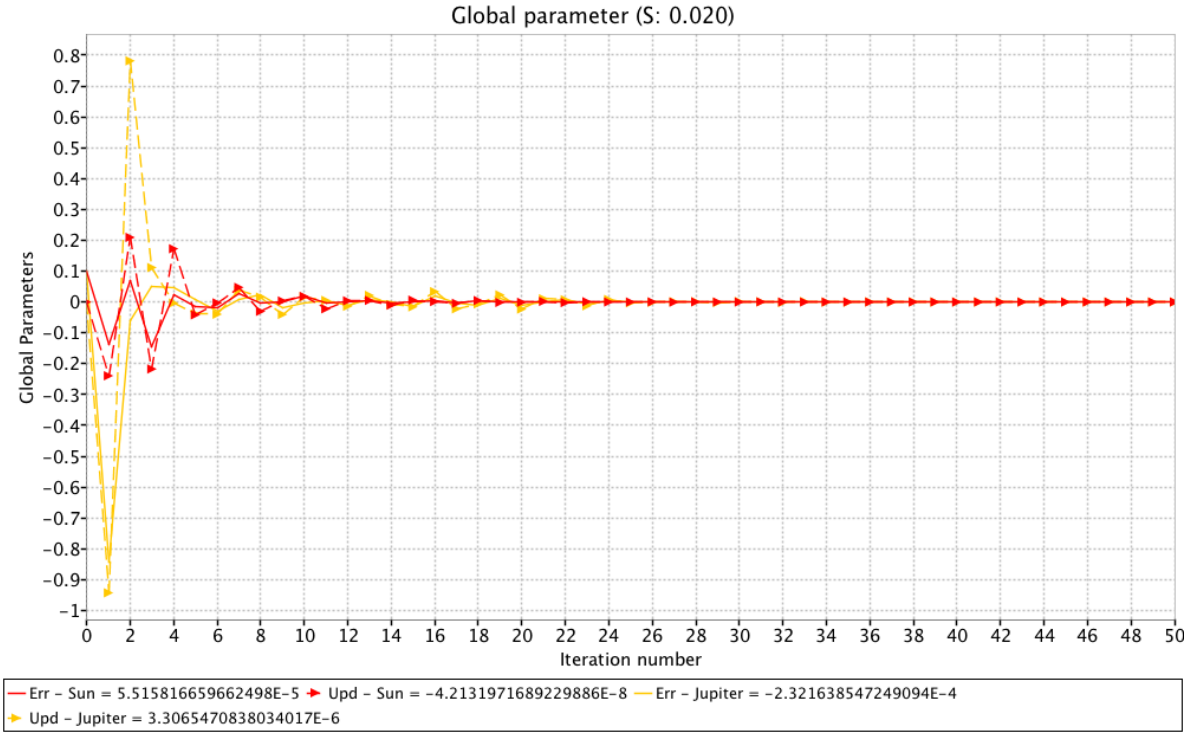

Figure 17: Convergence plot for the global parameters, in red (→) the error in PPN γ of the Sun and in yellow (→) the error in PPN γ of Jupiter, original AGIS implementation. The numbers in the box at the bottom of the graphs indicate the values at the end of iteration 50. (Plot generated using AGISLab)

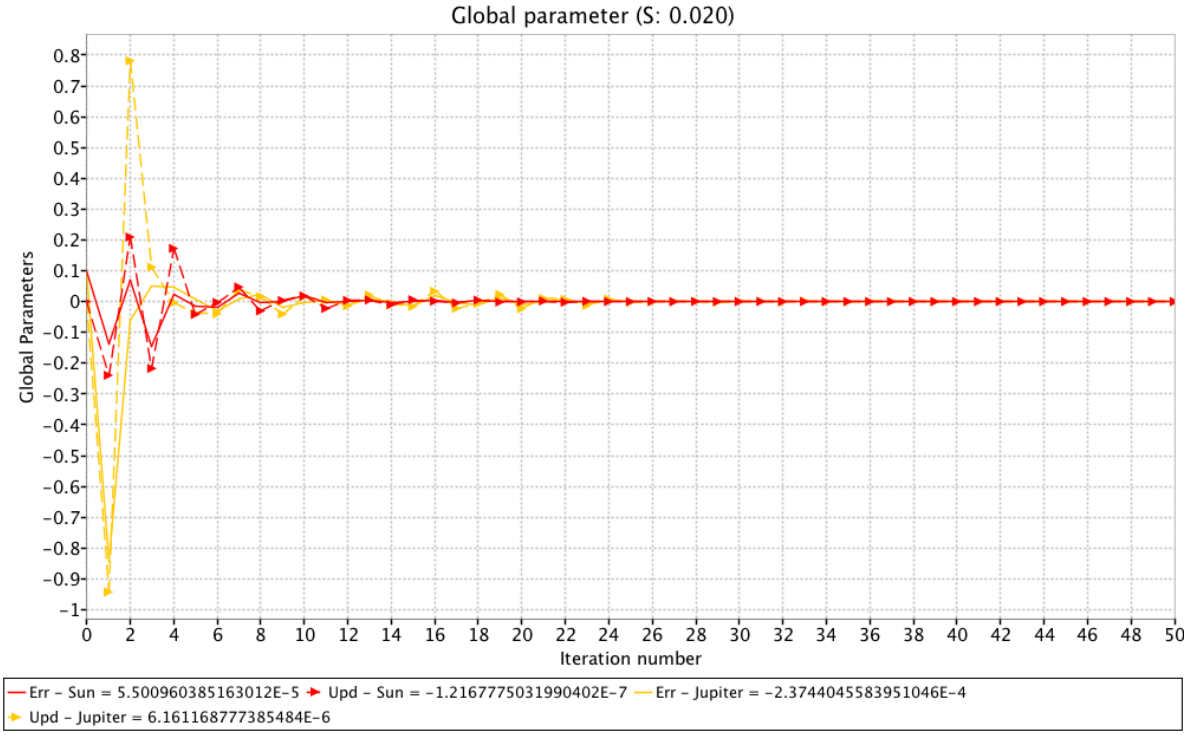

Figure 18: Convergence plot for the global parameters, in red (→) the error in PPN γ of the Sun and in yellow (→) the error in PPN γ of Jupiter, revised implementation using the formula from Crosta and Mignard to monopole order, and the derivative formula (61). The numbers in the box at the bottom of the graphs indicate the values at the end of iteration 50. (Plot generated using AGISLab)

4 Conclusion

We have shown that the formalism we wish to implement in the tests and in AGISLab gives coherent results. Our first tests in AGISLab agree with the results obtained with the previously implemented formalism. The main limitation of our results here is the size of the simulation. Indeed it is a small run with only 20 000 stars. It does allow to establish that the setup converges. The results however are only lower bounds on Gaia's possible performance in measuring PPN γ for both the Sun and Jupiter.

The quadrupole effect is more difficult to detect as it is weaker and multiple observations of the field in the vicinity of Jupiter are necessary to separate the monopole and quadrupole effects. It is also made harder to detect by the saturation of the CCDs by Jupiter. The impossibility to observe in the vicinity is expected to present the greatest constraint for its detection. The effect is strongest for small separations from Jupiter, but it is estimated that for most stars (G>13.5) within 5 arcsec of the planet's limb no measurement data can be obtained. [Martin Fleitas et al., 2011].

It has been pointed out by Zschocke and Klioner [2011] that it is not necessary to compute Jupiter's quadrupole deflection and derivatives for stars all over the sky. Due to the smallness of the effect far away from Jupiter, it is likely to be drowned in noise. In our simulations of about 100 thousand stars however this is not a big concern. For larger runs a filter for stars at large angles from Jupiter could be implemented in AGISLab.

Our work on this model of general relativity in the context of Gaia, AGIS and AGISLab will allow to demonstrate the feasibility of this calculation, and will be of use for the integration of Gaia's baseline relativity model, GREM, into AGISLab [Klioner, 2003, 2008]. We hope that the comparison of the results of this model with those obtained by more detailed relativistic models such as GREM and RAMOD, will give greater insight into the possible performance of Gaia.

Another effect that can be studied is the correlation of the errors in PPN γ (of the Sun) and basic angle variations. This correlation may potentially be broken by including light deflection effects from the planets. The avoidance of (large) basic angle variations is an essential requirement of the mission, their amplitude will be constantly monitored. However they cannot be completely avoided and the effect even of small variations is being studied by DPAC [Hobbs and Lindegren, 2010]. An interesting extension of this project would be to study how the estimation of plentary deflection can improve the robustness of Gaia to these variations of the basic angle.

In a second report we will describe the implementation of relativistic model in AGISLab and discuss the effects of monopole gravitational light deflection in the data reduction for Gaia.

Acknowledgements

I would like to thank my supervisor David Hobbs for proposing this exciting project and for his help along the way. His encouragement, his scientific advice, his effort and helpful implication have been invaluable. I am also grateful to my co-supervisor Lennart Lindegren for his accurate explanations and his comments which were always relevant, illuminating and demystifying. My thanks also go to Berry, Chris and Daniel for casual and helpful discussions about Gaia and AGIS.
In addition, I would like to express my gratitude to Ross Church and Johan Bijnens for valuable comments and discussions.

I would like to express my gratitude to Françoise Loytier and Sara Vilotti Pereira who have been of invaluable help during my stay in Lund. I would like to acknowledge also the help of Jean-Claude Mollier, my coordinator in Toulouse, who encouraged me to pursue physics.
My gratitude also goes to Melvyn B. Davies, the staff and students at Lund Observatory and Lund University for having made me feel welcome and the role they have played in my education.
I am grateful for the support of the *Agence pour l'enseigment français à l'étranger* over the five years of my studies in *classes préparatoires* and the *Ecole d'Ingénieur*.

To Alexey, Xinyi, Thomas, Charles, Sophia and Kristina go my sincere thanks for all the long conversations we have had about science, life and everything. They have been eye opening and I would not want to miss them. To all my friends go my thanks for cheering me up and for their understanding.
Most of all I would like to thank my family. My parents Elisabeth and Toni, and Ria and Werner for their support, their reliable advice, their kind words and for believing in me at all times.

References

Milton Abramowitz and Irene A. Stegun. *Handbook of Mathematical Functions with Formulas, Graphs, and Mathematical Tables*. Dover, New York, ninth dover printing, tenth gpo printing edition, 1964.

E.G. Adelberger. New tests of Einstein's equivalence principle and Newton's inverse-square law. *Class. Quantum Grav.*, 18:2397–2405, 2001. doi: 10.1088/0264-9381/18/13/302.

S. Baeßler, B.R. Heckel, E.G. Adelberger, J.H. Gundlach, U. Schmidt, and H.E. Swanson. Improved Test of the Equivalence Principle for Gravitational Self-Energy. *Phys. Rev. Lett.*, 83:3585–3588, 1999. doi: 10.1103/PhysRevLett.83.3585.

U. Bastian. Reference Systems, Conventions and Notations for Gaia. *Gaia Technical Note*, 07 2007.

B. Bertotti, L. Iess, and P. Tortora. A test of general relativity using radio links with the Cassini spacecraft. *Nature*, 425(6956):374–376, 2003. ISSN 0028-0836. doi: 10.1038/nature01997. URL `http://dx.doi.org/10.1038/nature01997`.

A. Bombrun, L. Lindegren, B. Holl, and S. Jordan. Complexity of the Gaia astrometric least-squares problem and the (non-)feasibility of a direct solution method. A&A, 516:A77+, June 2010. doi: 10.1051/0004-6361/200913503.

M. Crosta. Tracing light propagation to the intrinsic accuracy of space-time geometry. *ArXiv e-prints*, December 2010.

M. Crosta and A. Vecchiato. Gaia relativistic astrometric models. I. Proper stellar direction and aberration. A&A, 509:A37+, January 2010. doi: 10.1051/0004-6361/200912691.

M. T. Crosta and F. Mignard. Microarcsecond light bending by Jupiter. *Classical and Quantum Gravity*, 23:4853–4871, August 2006. doi: 10.1088/0264-9381/23/15/006.

Jos de Bruijne. Along- and across-scan location-estimation performance, 07 2009. URL `http://www.rssd.esa.int/llink/livelink/open/2913726`.

ESA Science Team. Gaia information sheets. ESA Gaia mission website, 2010. `http://www.rssd.esa.int/index.php?project=GAIA&page=Info_sheets_overview`.

A. Fienga, H. Manche, J. Laskar, and M. Gastineau. INPOP06: a new numerical planetary ephemeris. A&A, 477:315–327, January 2008. doi: 10.1051/0004-6361:20066607.

E. B. Fomalont and R. A. Sramek. Measurements of the solar gravitational deflection of radio waves in agreement with general relativity. *Physical Review Letters*, 36:1475–1478, June 1976. doi: 10.1103/PhysRevLett.36.1475.

M. Froeschle, F. Mignard, and F. Arenou. Determination of the PPN Parameter gamma with the HIPPARCOS Data. In R. M. Bonnet, E. Hög, P. L. Bernacca, L. Emiliani, A. Blaauw, C. Turon, J. Kovalevsky, L. Lindegren, H. Hassan, M. Bouffard, B. Strim, D. Heger, M. A. C. Perryman, & L. Woltjer, editor, *Hipparcos - Venice '97*, volume 402 of *ESA Special Publication*, pages 49–52, August 1997.

B. Guinot. Résolution A4(1991), Union Astronomique Internationale, sur les systèmes de réferencé: echelles de temps. In *Journées 1992: Systèmes de référence spatio-temporels*, pages 12–21, 1992.

D. Hestroffer, S. Mouret, F. Mignard, P. Tanga, and J. Berthier. Gaia and the asteroids: Local test of GR. In S. A. Klioner, P. K. Seidelmann, & M. H. Soffel, editor, *IAU Symposium*, volume 261 of *IAU Symposium*, pages 325–330, January 2010. doi: 10.1017/S1743921309990585.

D. Hobbs and L. Lindegren. Impact of systematic basic angle variations on the parallax zero point, February 2010. URL `http://www.rssd.esa.int/llink/livelink/open/3010458`.

D. Hobbs, B. Holl, L. Lindegren, F. Raison, S. Klioner, and A. Butkevich. Determining PPN γ with Gaia's astrometric core solution. In S. A. Klioner, P. K. Seidelmann, & M. H. Soffel, editor, *IAU Symposium*, volume 261 of *IAU Symposium*, pages 315–319, January 2010. doi: 10.1017/S1743921309990561.

B. Holl, D. Hobbs, and L. Lindegren. Spatial correlations in the Gaia astrometric solution. In S. A. Klioner, P. K. Seidelmann, & M. H. Soffel, editor, *IAU Symposium*, volume 261 of *IAU Symposium*, pages 320–324, January 2010. doi: 10.1017/S1743921309990573.

G. Jasniewicz, F. Crifo, C. Soubiran, D. Hestroffer, A. Siebert, L. Veltz, L. Bigot, L. Chemin, P. David, A. Guerrier, D. Katz, H.-G. Ludwig, P. Richard, F. Royer, P. Sartoretti, and S. Udry. Radial Velocity Standard Stars for the Gaia RVS. In *EAS Publications Series*, volume 45 of *EAS Publications Series*, pages 195–200, February 2011. doi: 10.1051/eas/1045033.

C. Jordi, M. Gebran, J. M. Carrasco, J. de Bruijne, H. Voss, C. Fabricius, J. Knude, A. Vallenari, R. Kohley, and A. Mora. Gaia broad band photometry. A&A, 523:A48+, November 2010. doi: 10.1051/0004-6361/201015441.

S. A. Klioner. A Practical Relativistic Model for Microarcsecond Astrometry in Space. AJ, 125:1580–1597, March 2003.

S. A. Klioner. Physically adequate proper reference system of a test observer and relativistic description of the GAIA attitude. *Phys. Rev. D*, 69(12):124001–+, June 2004. doi: 10.1103/PhysRevD.69.124001.

S. A. Klioner. Gaia relativity model: concise description. *Gaia Technical Note*, 2008.

S. M. Kopeikin and V. V. Makarov. Gravitational bending of light by planetary multipoles and its measurement with microarcsecond astronomical interferometers. Phys. Rev. D, 75 (6):062002–+, March 2007. doi: 10.1103/PhysRevD.75.062002.

J. Kovalevsky. *Modern Astrometry*. 2002.

U. Lammers and L. Lindegren. News on Seeking Gaia's Astrometric Core Solution with AGIS. In *EAS Publications Series*, volume 45 of *EAS Publications Series*, pages 123–126, February 2011. doi: 10.1051/eas/1045021.

L. D. Landau and E. M. Lifshitz. *The classical theory of fields*. 1975.

M.G. Lattanzi and M.-T. Crosta. Implementation of the quadrupole deflection experiment in DPAC (GA REQ), November 2009. URL `http://www.rssd.esa.int/llink/livelink/open/2941668`.

Adrien-Marie Le Gendre. Recherches sur l'attraction des sphéroïdes homogènes (*Studies on the attraction of homogeneous spheroids*). *Mémoires de Mathématiques et de Physique, présentés à l'Académie royale des sciences (Paris) par sçavants étrangers*, 10:411–435, 1782.

A.P. Lightman and D.L. Lee. Restricted proof that the weak equivalence principle implies the Einstein equivalence principle. *Phys. Rev. D*, 8:364–376, 1973.

L. Lindegren. Proposed prototype processes for the GAIA Global Iterative Solution, March 2001. URL `http://www.rssd.esa.int/llink/livelink/open/357825`.

L. Lindegren and U. Bastian. Basic principles of scanning space astrometry. In *EAS Publications Series*, volume 45 of *EAS Publications Series*, pages 109–114, February 2011. doi: 10.1051/eas/1045018.

L. Lindegren, E. Hog, F. van Leeuwen, C. A. Murray, D. W. Evans, M. J. Penston, M. A. C. Perryman, C. Petersen, N. Ramamani, and M. A. J. Snijders. The NDAC HIPPARCOS data analysis consortium - Overview of the reduction methods. A&A, 258:18–30, May 1992.

L. Lindegren, U. Lammers, D. Hobbs, W. O'Mullane, U. Bastian, and J. Hernandez. The astrometric core solution for the Gaia mission, Overview of models, algorithms and software implementation. submitted August 2011.

J.M. Martin Fleitas, A. Mora, F. Raison, et al. VPU. Object detectability near bright extended sources. The Jupiter case, February 2011. URL `http://www.rssd.esa.int/llink/livelink/open/3061697`.

F. Mignard. Fundamental Physics with GAIA. In O. Bienayme & C. Turon, editor, *EAS Publications Series*, volume 2 of *EAS Publications Series*, pages 107–121, 2002.

K.L. Nordtvedt Jr. Equivalence Principle for Massive Bodies. I. Phenomenology. *Phys. Rev.*, 169:1014–1016, 1968. doi: 10.1103/PhysRev.169.1014.

M. Perryman. *The Making of History's Greatest Star Map*. 2010.

T. Prusti. General status of the Gaia mission and expected performance. In *EAS Publications Series*, volume 45 of *EAS Publications Series*, pages 9–14, February 2011. doi: 10.1051/eas/1045002.

H. Rickman. Transactions of the International Astronomical Union Proceedings of the Twenty-Fourth General Assembly. *Transactions of the International Astronomical Union, Series B*, 24, 2001.

I.W. Roxburgh. Gravitational multipole moments of the Sun determined from helioseismic estimates of the internal structure and rotation. *Astron. Astrophys.*, 377:688–690, 2001. doi: 10.1051/0004-6361:20011104.

P. Schneider, J. Ehlers, and E. E. Falco. *Gravitational Lenses*. 1992.

R. U. Sexl and H. Sexl. *White dwarfs-black holes: an introduction to relativistic astrophysics*. 1979.

M. Soffel, S. A. Klioner, G. Petit, P. Wolf, S. M. Kopeikin, P. Bretagnon, V. A. Brumberg, N. Capitaine, T. Damour, T. Fukushima, B. Guinot, T.-Y. Huang, L. Lindegren, C. Ma, K. Nordtvedt, J. C. Ries, P. K. Seidelmann, D. Vokrouhlický, C. M. Will, and C. Xu. The IAU 2000 Resolutions for Astrometry, Celestial Mechanics, and Metrology in the Relativistic Framework: Explanatory Supplement. AJ, 126:2687–2706, December 2003. doi: 10.1086/378162.

J. Soldner. Über die Ablenkung eines Lichstrahls von seiner geradlinigen Bewegung, durch die Attraktion eines Weltkörpers, an welchem er nahe vorbei geht (*On the deviation of a light ray*). *Berliner astronomisches Jahrbuch*, page 161, 1801. URL `http://books.google.com/books?id=PN43AAAAMAAJ`.

Y. Su, B.R. Heckel, E.G. Adelberger, J.H. Gundlach, M. Harris, G.L. Smith, and H.E. Swanson. New tests of the universality of free fall. *Phys. Rev. D*, 50:3614–3636, 1994. doi: 10.1103/PhysRevD.50.3614.

J. M. Weisberg and J. H. Taylor. The Relativistic Binary Pulsar B1913+16: Thirty Years of Observations and Analysis. In F. A. Rasio & I. H. Stairs, editor, *Binary Radio Pulsars*, volume 328 of *Astronomical Society of the Pacific Conference Series*, pages 25–+, July 2005.

Clifford M. Will. The Confrontation between General Relativity and Experiment. *Living Reviews in Relativity*, 9(3), 2006. URL `http://www.livingreviews.org/lrr-2006-3`.

Clifford M. Will. On the unreasonable effectiveness of the post-Newtonian approximation in gravitational physics. *Proceedings of the National Academy of Sciences*, 2011. doi: 10.1073/pnas.1103127108. URL `http://www.pnas.org/content/early/2011/03/28/1103127108.abstract`.

C.M. Will. *Theory and Experiment in Gravitational Physics*. Cambridge University Press, Cambridge; New York, 2nd edition, 1993.

S. Zschocke and S. A. Klioner. On the efficient computation of the quadrupole light deflection. *Classical and Quantum Gravity*, 28(1):015009–+, January 2011. doi: 10.1088/0264-9381/28/1/015009.

A Acronyms and Notations

Abbreviation	Meaning
AC	across-scan
AGIS	Astrometric Global Iterative Solution
AL	along-scan
as or $''$	second of arc or arcsecond (arcsec), 1 part in 3600 of one degree
AU	astronomical unit
BCRS	Barycentric Reference System
ESAC	European Space Astronomy Centre (ESAC), near Madrid
CoMRS	Center-of-Mass Reference System (of Gaia)
FL	First-Look
FoV	field of view
Gaia	(formerly) Global Astrometric Interferometer for Astrophysics
GCRS	Geocentric Reference System
Hipparcos	High Precision Parallax Collecting Satellite
IAU	International Astronomical Union
ICRS	International Celestial Reference System
ICRF	International Celestial Reference Frame
IDT	Initial Data Treatment
IMCCE	Institut de Mécanique Céleste et de Calcul des Éphémérides, Paris
ISO	International Organisation for Standardization, Geneva
JD	Julian Date; a notation for time
JPL	Jet Propulsion Laboratory, NASA, Pasadena
ODAS	One Day Astrometric Solution
PPN	parametrized post-Newtonian
μarcsec	micro arcsecond
QEF	quadrupole efficiency factor

Table 9: The listing of the acronyms used in this work.

B Tensor equations

B.1 Covariant derivative and Christoffel symbols

For partial derivatives we use the following notation :

$$\partial_\beta A_\alpha \quad := \quad \frac{\partial}{\partial x^\beta} A_\alpha \tag{66}$$

Some authors also use the notation $A_{\alpha\,,\beta} = \partial_\beta A_\alpha$ which we have avoided here. In tensorial equations, we use the Einstein summation convention. Greek indices range from 0 to 3, latin indices from 1 to 3. The Christoffel symbols $\Gamma^\alpha_{\beta\gamma}$ (also called connection coefficients): are defined by (67). Relation (68) relates them to the metric tensor.

$$\Gamma^\alpha_{\beta\gamma} \quad = \quad -\,\partial_\beta \bar{x}^\mu \partial_\gamma \bar{x}^\nu \partial_{\bar{\mu}} \partial_{\bar{\nu}} x^\alpha \tag{67}$$

$$\Gamma^\alpha_{\beta\gamma} \quad = \quad \frac{1}{2}\, g_{\nu\mu}\,(\,\partial_\beta g_{\mu\alpha} + \partial_\alpha g_{\mu\beta} - \partial_\mu g_{\alpha\beta}\,) \tag{68}$$

We define the covariant derivative of a covariant tensor A_α by

$$A_{\alpha;\,\beta} \quad = \quad \partial_\beta A_\alpha + \Gamma^\nu_{\alpha\beta} A_\nu \tag{69}$$

B.2 Riemann and Einstein tensors

The Riemann curvature tensor $R^{\mu}_{\nu\alpha\beta}$, which is a function of the Christoffel symbols and therefore of the metric itself.

$$R^{\mu}_{\nu\alpha\beta} = \partial_{\alpha}\Gamma^{\mu}_{\nu\beta} - \partial_{\beta}\Gamma^{\mu}_{\nu\alpha} + \Gamma^{\mu}_{\gamma\alpha}\Gamma^{\gamma}_{\nu\beta} - \Gamma^{\mu}_{\gamma\beta}\Gamma^{\gamma}_{\nu\alpha} \tag{70}$$

as given in Will [1993, section 3.2].
The Einstein tensor $G_{\mu\nu}$ is defined as:

$$G_{\mu\nu} = R_{\mu\nu} - \frac{1}{2}g_{\mu\nu}R \tag{71}$$

where $R_{\alpha\beta}$ and R are defined as contractions of the Riemann curvature tensor. The Ricci tensor is $R_{\alpha\beta} = R^{\nu}_{\alpha\nu\beta}$ and the Ricci scalar is $R = g^{\alpha\beta}R_{\alpha\beta}$.

B.3 Energy-momentum tensor

The energy momentum tensor appearing the in the field equations (5) will depend on the model of matter chosen. A fairly general example is given by [Will, 1993], where matter is modeled as a perfect fluid in which case:

$$T^{\mu\nu} = (\,\rho + \rho\Pi + p\,)\,u^{\mu}u^{\nu} + p\,g^{\mu\nu} \tag{72}$$

where the quantities are defined as follows:

- ρ is rest-mass–energy density of atoms in the fluid element,
- p is the isotropic pressure of the fluid,
- Π is the specific density of internal kinetic and thermal energy,
- $u^{\mu} = dx^{\mu}/d\tau$ is the four-velocity vector of the fluid element.

and τ is the separation between two space-time events:

$$d\tau^2 = \epsilon\, g^{\mu\nu}x^{\mu}x^{\nu} \tag{73}$$

$$\tau = \int_{Path:a\to b} d\tau \tag{74}$$

where $\epsilon = \pm 1$ is chosen so that $d\tau^2$ is positive. The separation between two events is called time-like if $\epsilon = -1$ and space-like otherwise. If $g^{\mu\nu}x^{\mu}x^{\nu} = 0$ the separation is called light-like, since light rays move along these null trajectories.

C Units

In this work we use SI units[14]. It is noteworthy that units are locally defined as "proper units" in a reference frame. The question of their use and interpretation in general relativistic context is discussed in the IAU resolution of 1991 Guinot [1992].

quantity	unit	value
G	$[m^3 kg^{-1} s^{-2}]$	$6.67428 \cdot 10^{-11}$
c	$[m\, s^{-1}]$	$2.99792458 \cdot 10^{8}$
a	$[m\, AU^{-1}]$	$1.49597870691 \cdot 10^{11}$

Table 10: Values of constants used in AGIS and AGISLab, provided by the Gaia Parameter Database (`http://gaia.esac.esa.int/gpdb`).

[14] *Système International* `http://www.bipm.org/en/si/`

D Legendre polynomials

The Legendre polynomials are given by the concise explicit expression (75):

$$P_n(y) = \frac{1}{2^n(n!)}\partial_y^n\left[\left(y^2-1\right)^n\right] \tag{75}$$

$$(n+1)P_{n+1}(y) = (2n+1)yP_n(y) - nP_{n-1}(y) \tag{76}$$

where n is a positive integer number. Relation (76) is called Bonnet's recursion formula.

These mathematical results can be found at `http://dlmf.nist.gov/` and Abramowitz and Stegun [1964] chapter 8.

The following are the first four polynomials which are used in the calculation in section 3.3.3.

$$P_0(y) = 1 \tag{77}$$
$$P_1(y) = y \tag{78}$$
$$P_2(y) = \frac{1}{2}\left(3y^2-1\right) \tag{79}$$
$$P_3(y) = \frac{1}{2}\left(5y^3-3y\right) \tag{80}$$

E The equations of the PPN formalism

The equations shown below in figures 19 and 20, are taken from Will [2006, p. 29 and 30]. They show the role of the PPN parameters in the metric, as well as the definitions of the metric potentials in terms of the matter variables and coordinates.

Box 2. The Parametrized Post-Newtonian formalism

Coordinate system:

The framework uses a nearly globally Lorentz coordinate system in which the coordinates are (t, x^1, x^2, x^3). Three-dimensional, Euclidean vector notation is used throughout. All coordinate arbitrariness ("gauge freedom") has been removed by specialization of the coordinates to the standard PPN gauge (TEGP 4.2 [281]). Units are chosen so that $G = c = 1$, where G is the physically measured Newtonian constant far from the solar system.

Matter variables:

- ρ: density of rest mass as measured in a local freely falling frame momentarily comoving with the gravitating matter.
- $v^i = (dx^i/dt)$: coordinate velocity of the matter.
- w^i: coordinate velocity of the PPN coordinate system relative to the mean rest-frame of the universe.
- p: pressure as measured in a local freely falling frame momentarily comoving with the matter.
- Π: internal energy per unit rest mass (it includes all forms of non-rest-mass, non-gravitational energy, e.g., energy of compression and thermal energy).

PPN parameters:

γ, β, ξ, α_1, α_2, α_3, ζ_1, ζ_2, ζ_3, ζ_4.

Metric:

$$
\begin{aligned}
g_{00} &= -1 + 2U - 2\beta U^2 - 2\xi\Phi_W + (2\gamma + 2 + \alpha_3 + \zeta_1 - 2\xi)\Phi_1 + 2(3\gamma - 2\beta + 1 + \zeta_2 + \xi)\Phi_2 \\
&\quad + 2(1 + \zeta_3)\Phi_3 + 2(3\gamma + 3\zeta_4 - 2\xi)\Phi_4 - (\zeta_1 - 2\xi)\mathcal{A} - (\alpha_1 - \alpha_2 - \alpha_3)w^2 U - \alpha_2 w^i w^j U_{ij} \\
&\quad + (2\alpha_3 - \alpha_1)w^i V_i + \mathcal{O}(\epsilon^3), \\
g_{0i} &= -\frac{1}{2}(4\gamma + 3 + \alpha_1 - \alpha_2 + \zeta_1 - 2\xi)V_i - \frac{1}{2}(1 + \alpha_2 - \zeta_1 + 2\xi)W_i - \frac{1}{2}(\alpha_1 - 2\alpha_2)w^i U \\
&\quad - \alpha_2 w^j U_{ij} + \mathcal{O}(\epsilon^{5/2}), \\
g_{ij} &= (1 + 2\gamma U)\delta_{ij} + \mathcal{O}(\epsilon^2).
\end{aligned}
$$

Figure 19: The full equations of the PPN formalism as given in [Will, 2006]. (TEGP 4.2 refers to [Will, 1993] section 4.2)

Metric potentials:

$$
\begin{aligned}
U &= \int \frac{\rho'}{|\mathbf{x}-\mathbf{x}'|}\, d^3x', \\
U_{ij} &= \int \frac{\rho'(x-x')_i(x-x')_j}{|\mathbf{x}-\mathbf{x}'|^3}\, d^3x', \\
\Phi_W &= \int \frac{\rho'\rho''(\mathbf{x}-\mathbf{x}')}{|\mathbf{x}-\mathbf{x}'|^3} \cdot \left(\frac{\mathbf{x}'-\mathbf{x}''}{|\mathbf{x}-\mathbf{x}''|} - \frac{\mathbf{x}-\mathbf{x}''}{|\mathbf{x}'-\mathbf{x}''|} \right) d^3x'\, d^3x'', \\
\mathcal{A} &= \int \frac{\rho'[\mathbf{v}'\cdot(\mathbf{x}-\mathbf{x}')]^2}{|\mathbf{x}-\mathbf{x}'|^3}\, d^3x', \\
\Phi_1 &= \int \frac{\rho' v'^2}{|\mathbf{x}-\mathbf{x}'|}\, d^3x', \\
\Phi_2 &= \int \frac{\rho' U'}{|\mathbf{x}-\mathbf{x}'|}\, d^3x', \\
\Phi_3 &= \int \frac{\rho'\Pi'}{|\mathbf{x}-\mathbf{x}'|}\, d^3x', \\
\Phi_4 &= \int \frac{p'}{|\mathbf{x}-\mathbf{x}'|}\, d^3x', \\
V_i &= \int \frac{\rho' v'_i}{|\mathbf{x}-\mathbf{x}'|}\, d^3x', \\
W_i &= \int \frac{\rho'[\mathbf{v}'\cdot(\mathbf{x}-\mathbf{x}')](x-x')_i}{|\mathbf{x}-\mathbf{x}'|^3}\, d^3x'.
\end{aligned}
$$

Stress–energy tensor (perfect fluid):

$$
\begin{aligned}
T^{00} &= \rho(1+\Pi+v^2+2U), \\
T^{0i} &= \rho v^i \left(1+\Pi+v^2+2U+\frac{p}{\rho}\right), \\
T^{ij} &= \rho v^i v^j \left(1+\Pi+v^2+2U+\frac{p}{\rho}\right) + p\delta^{ij}(1-2\gamma U).
\end{aligned}
$$

Equations of motion:

- Stressed matter: $T^{\mu\nu}{}_{;\nu} = 0$.
- Test bodies: $\dfrac{d^2x^\mu}{d\lambda^2} + \Gamma^\mu{}_{\nu\lambda}\dfrac{dx^\nu}{d\lambda}\dfrac{dx^\lambda}{d\lambda} = 0$.
- Maxwell's equations: $F^{\mu\nu}{}_{;\nu} = 4\pi J^\mu, \qquad F_{\mu\nu} = A_{\nu;\mu} - A_{\mu;\nu}$.

Figure 20: The full equations of the PPN formalism as given in [Will, 2006], continued.